EXPRESSION AND PURIFICATION OF *LUCINA PECTINATA* RECOMBINANT HEMOGLOBIN II AND THE EFFECT OF THE OXYGEN AFFINITY ON THE HEME POCKET

By
Wilmarie Lorenzo-González

A thesis proposal submitted in partial fulfillment of the requirements for the degree of

MASTER OF SCIENCE
in
CHEMISTRY

UNIVERSITY OF PUERTO RICO
MAYAGÜEZ CAMPUS
2009

Approved by**:**

---	---
Carmen A. Vega, Ph.D. Member, Graduate Committee	Date
---	---
Carmen L. Cadilla, Ph.D. Member, Graduate Committee	Date
---	---
Juan López-Garriga, Ph.D. President, Graduate Committee	Date
---	---
Dallas E. Alston, Ph.D. Graduate Student Representative	Date
---	---
Francis Patron, Ph.D. Chairperson, Chemistry Department	Date

Abstract

Lucina pectinata is a bivalve mollusk that inhabits sulfide rich sediments along, the west coast of Puerto Rico. This clam contains three hemoglobins that deliver and transport oxygen (HbII and III) and hydrogen sulfide (HbI) to chemoautotrophic bacteria. The HbII is an oxygen reactive protein in which the oxygen is anchored to the heme through H-bonds with Tyr30 (B10) and Gln65 (E7) being responsible for the extremely low oxygen dissociation rate (0.11 s^{-1}). A previous experiment showed that HbII is resistant to H_2O_2 and NO oxidation characteristics useful for the development of oxygen carrier derivatives. However, it is necessary to improve oxygen binding and induce allosteric properties of HbII. This was achieved through site-directed mutagenesis of HbII. Here, we report that recombinant HbII (rHbII) expression in bacteria was obtained after induction in a time course of 3-4 hours and the maximum rHbII protein yield obtained was 134.72 mg/L using the pET28 expression vector transformed in BLi5 cells. The optimal expression condition occurred when the induction was performed at 30 °C and when the terrific broth medium was supplemented with 1 mM IPTG and 60 µg/mL hemin chloride. To monitor the expression, we extracted the proteins and purified the rHbII using a metal resin. The protein product was analyzed using UV-Vis spectroscopy; the concentration of rHbII protein was determined using the molar extinction coefficient of 129 $mM^{-1}cm^{-1}$ at 414 nm for the oxy-rHbII. Functional characterization of the rHbII was performed with the formation of oxy, deoxy, and CO complex. In addition, kinetics measurements of O_2 affinity were performed using a Stopped-flow system and the dissociation rate constant value obtained was 0.0526 s^{-1}, whereas the association rate constant was 0.19 x 10^6 $M^{-1}s^{-1}$. These values were similar to the native HbII dissociation and association constants, 0.11 s^{-1} and 0.390 x 10^6 $M^{-1}s^{-1}$, respectively.

Resumen

Lucina pectinata es un molusco bivalvo que habita en sedimentos ricos en sulfuro; en la costa oeste de Puerto Rico. Esta almeja contiene tres hemoglobinas, las cuales entregan y transportan oxígeno (hemoglobina II y III) y sulfuro de hidrógeno (hemoglobina I) a una bacteria quimioautótrofa. La hemoglobina II es una proteína reactiva a oxígeno en la cual este se halla enlazado al grupo hemo a través de puentes de hidrógeno con Tyr30 (B10) y Gln65 (E7). Esto resulta en que la velocidad de disociación de oxígeno sea extremadamente baja (0.11 s^{-1}). Trabajos previos han demostrado que HbII es muy resistente a la oxidación de H_2O_2 y NO, características típicas para el desarrollo de derivados de transportadores de oxígeno. Sin embargo, es necesario mejorar el enlazamiento de oxígeno e inducir propiedades alostéricas de HbII. Esto es logrado a través de mutaciones dirigidas de HbII. Aquí nosotros reportamos la expresión de la hemoglobina II recombinante se obtuvo luego de una inducción en un tiempo de 3-4 horas y el rendimiento máximo de proteína obtenido fue 134.72 mg/L utilizando el vector de expresión pET28 transformado en las bacterias BLi5. Las condiciones óptimas de expresión ocurrieron cuando la inducción se llevo a cabo a 30 °C y el medio "Terrific Broth" fue suplementado con 1 mM IPTG, 60 µg/mL cloruro de hemo y 1% glucosa. Para monitorear la expresión, se extrajeron las proteínas, y además se purificó rHbII con una resina de afinidad metálica para obtener rHbII. El producto fue analizado utilizando un espectrofotómetro de UV-Vis y la concentración de la proteína de rHbII fue determinada utilizando el coeficiente de extinción molar de 129 $mM^{-1}cm^{-1}$ a 414 nm para rHbII en su forma oxy. La caracterización funcional de rHbII fue llevada a cabo con la formación de complejos con O_2 y CO. Además, se realizaron medidas cinéticas para determinar la afinidad con O_2 utilizando un sistema de "Stopped Flow". El valor obtenido de la constante de disociación fue 0.0526 s^{-1} y 0.19 x 10^6 M^-

$^{1}s^{-1}$ para la constante de asociación. Estos valores son muy similares a las constantes de disociación y asociación de HbII en su forma nativa, 0.11 s^{-1} y 0.390 x 10^{6} $M^{-1}s^{-1}$, respectivamente.

To my parents Wilson Lorenzo and Luz M. González,
for being my inspiration and motivation.

ACKNOWLEDGEMENTS

First, I would like to thank God for giving me the strength to complete this project. To my family, the most important people in my life, my dad, Wilson Lorenzo, my mother, Luz M. González and my brother Wilson M. Lorenzo for their unconditional support, and love; I never will have made it without you.

Second, I want to thank Dr. Juan López-Garriga, my thesis advisor, for his support throughout this period of my life. Also I would like to thank my thesis committee, Dr. Carmen L. Cadilla and Dr. Carmen Vega, for all their help during my graduate student years.

Also I would like to thank Ruth Pietri and Cacimar Ramos for their support and the time spent to help me whenever it was needed. To Josiris Rodríguez, Carlos Ruiz, Carlos Nieves, and Rafael Estremera: thanks for the motivation, support, and friendship. Thanks to my closest friends, Debra Ramos, Idaines Feliciano, Rosalie Ramos, Samirah Mercado, Ismael Badillo, Christian O. Furseth, Omar Rivera, and Edward Camacho for their unconditional help and emotional support. And a special gratefulness to Héctor I. Areizaga for being at my side during these three years, for his patience, support, motivation, unconditional help and love.

Finally, thanks to the Chemistry Department at the University of Puerto Rico in Mayaguez and the Graduate and Undergraduate Students Enhancing Science and Technology in K-12 Schools (GUEST K-12) Program for their financial support.

Table of Contents

Abstract ii

Resumen iii

Acknowledgements vii

List of Symbols and Abbreviations x

List of Tables xii

List of Figures xiii

1. Introduction

1.1 Hemoglobins 1

1.2 Blood Substitutes 3

1.3 Hemoglobin II of *Lucina pectinata* 12

1.4 Objectives 16

2. Materials and Methods

2.1 Construction of rHbII into pET28 (a+) vector 17

2.2 Preparation of BLi5 and BL21 Competent Cells 17

2.3 Transformation of pET28 (a+) vector in the BLi5 Cells 19

2.4 Pilot Expression 20

2.5 High-level Expression of rHbII in *E. coli* 20

2.6 Cell lysate and Isolation of the Recombinant HbII Protein 23

2.7 Purification of rHbII 24

2.8 Purity and Concentration of Recombinant HbII 24

2.9 Formation of the Deoxy and Carbon Monoxide Complex of Recombinant HbII 27

2.10 Formation of the Met-hydroxide and met-acid Complex of Recombinant HbII 27

2.11 Kinetics of the reactions of rHbII with O_2 27

2.11.1 Determination of the Affinity Constant (k_{on}) 28

2.11.2 Determination of the Dissociation Affinity Constant (k_{off}) 29

2.12 Determination of the Autoxidation Constant (k_{ox}) 29

3. Results and Discusion

3.1 Recombinant HbII Transformation 31

3.2 Recombinant HbII Expression

3.2.1 Effect of the time induction during the rHbII expression 33

3.2.2 Effect of the temperature in the protein yield 36

3.2.3 Effect of the bacterial strains: BL21 and BLi5 *E. coli* strains 38

3.2.4 Overexpression of rHbII 40

3.3 Purification of the expressed protein 40

3.4 Reaction of rHbII with ligands (O_2, CO) 42

3.5 Formation of the met-hydroxide and met-aquo Complex of rHbII 50

3.6 Kinetics analysis of rHbII with O_2 54

4 Conclusions 68

Reference 69

List of Symbols and Abbreviations

Bp	Base pairs
BV	Bed volume
cDNA	Complementary deoxyribonucleic acid
CN^-	Cyanide
CO	Carbon monoxide
Cys	Cysteine
E. coli	Escherichia coli
Fe	Iron
Fe^{+2}	Ferrous iron
Fe^{+3}	Ferric iron
Fe^{IV}=O $Por^{+\cdot}$	Porphyrin π-cation radical ferryl compound I
Fe^{IV}=O	Ferryl compound II
FPLC	Fast protein liquid chromatography
Gln	Glutamine
HbA_0	Human hemoglobin
Hbs	Hemoglobins
HbI	Hemoglobin I from *Lucina pectinata*
HbII	Hemoglobin II from *Lucina pectinata*
HbIII	Hemoglobin III from *Lucina pectinata*
HbCO	Carboxy hemoglobin
HbO_2	Oxy hemoglobin
His	Histidine
H_2S	Hydrogen sulfide
H_2O_2	Hydrogen peroxide
IPTG	Isopropyl-1-thio-β-D-galactopyranoside
kDa	kilodaltons
k_{on}	Kinetics rate constant for association
k_{off}	Kinetics rate constant for dissociation

k_{ox}	Kinetics rate constant for autoxidation
L. pectinata	*Lucina pectinata*
LB	Luria broth
Mb	Myoglobin
NO	Nitric oxide
O_2	Oxygen
OD_{600}	Optical density at 600nm
rHbII	Recombinant hemoglobin II
SDS-PAGE	Sodium dodecyl sulfate-polyacrylamide gel electrophoresis
SOC	Super optimal broth with Catabolite repression
TB	Terrific broth
Tyr	Tyrosine
UV-Vis	Ultraviolet-Visible
wtHbII	Wild type hemoglobin II

Table List

Tables		Page
1.1	Different types of blood substitutes and the hemoglobin structural modifications to maintain the tetramer structure.	8
1.2	Different types of blood substitutes and their adverse effects	10
2.1	Spectral properties of the HbII complex from *Lucina pectinata*	26
3.1	Protein yield of rHbII in *E. coli* BL21 and BLi5 cells at different induction time.	35
3.2	Protein yield of rHbII in *E. coli* BL21 and BLi5 cells at different temperature of induction.	38
3.3	Protein yield of rHbII in *E. coli* BL21 and BLi5 cells at different parameters of expression.	38
3.4	Summary of the spectral properties obtained for the formation of the rHbII complex with the different ligands.	46
3.5	Values of the pseudo first order rate constant, *k'*, obtained from the first order exponential decay analysis for HbII at different O_2 concentrations.	62
3.6	Summary of the first order exponential decay analysis for wtHbII and rHbII and the k_{off} obtained.	64

Figure List

Figure		Page
1.1	Quaternary structure of hemoglobin (A). The hemoglobin consists of two α (blue) and two β (red) chains, each one attach to a heme prosthetic group (green). Each alpha-helix structure (B) is hydrogen-bonded to the amino acid between the –NH and –CO functional groups.	2
1.2	Schematic representation of the heme group (A) which contain a Fe iron in the center attached to four nitrogen of a heterocyclic macromolecule called a porphyrin. The heme group is attached to the globin by the histidine residue in the F8 helix (B).	4
1.3	Schematic diagram of the planar configuration adopts by the porphyrin ring in which in the oxygenated state (A) the heme group is planar and the Fe has a charge of Fe^{II}. Deoxygenated state in which (B) the heme group is nonplanar and the iron has a charge of Fe^{III}.	5
1.4	X-ray structure of Hemoglobin II of *Lucina pectinata.* HbII is an oxygen-binding hemoglobin and consists of two dimers of 163 amino acids. Each globin consist of six α-helices surrounding the central heme pocket, and two minor helical segments between the B and E helices	13
1.5	Diagram of the orientations of the distal residues of the wild type HbII from *L. pectinata* (A). In the distal site of the heme pocket HbII is GlnE7 instead of the classical histidine. The other surrounding amino acid residues are PheCD1, PheE11 and TyrB10. In the hydrogen bond network of HbII, the oxygen is tightly anchored to the heme through hydrogen bonds with TyrB10 and GlnE7 (B).	14
2.1	Diagram of the pET-28a(+) expression vector which contains a T7 promoter, 6x-His tags and a LacI gene. This plasmid confers resistance to kanamycin and has a single-cut directional cloning.	18

2.2 BioFlo 110 Modular Benchtop Fermentator of New Brunswick used to grow the BLi5 cells that produced the recombinant Hemoglobin II from *Lucina pectinata.* The Bioreactor includes a Primary Control Unit (PCU) and Power Controller to manage temperature, agitation, pH and pO_2. 22

2.3 Representation of the metal affinity chromatography of recombinant HbII using a FPLC. The first peak in the chromatogram represents the impurities in the sample. The second peak shows our protein (rHbII) in a mixture with imidazole and salts. 25

3.1 Agarose gel electrophoresis of the double enzymatic digestion with EcoRI and XhoI enzymes of the plasmid pET28(a+) containing the rHbII insert. Lane 1 and 10 contain the DNA ladder; lane 1 contains the 123 bp DNA ladder and lane 10 the 1 Kb DNA ladder. Lane 2-9 shows the expected bands of rHbII DNA after the double enzymatic digestion. 32

3.2 Sodium dodecyl sulfate polyacrylamide gel electrophoresis (SDS-PAGE) analysis for the detection of rHbII at different induction time. Lane 1 contains the SDS-PAGE standard and the lane 2-5 show the detection of rHbII, which has a theoretical molecular weight of 16,128 daltons, at different induction time. The lanes 2-3 show the rHbII detection when the induction time was less than 1.4 and lanes 4-5 when the induction was after the log phase (OD_{600} 1.4-2.0) 34

3.3 Sodium dodecyl sulfate polyacrylamide gel electrophoresis (SDS-PAGE) analysis for the detection of rHbII at different temperature of induction. Lanes 1 and 8 contain the SDS-PAGE standard and the lanes 2-7 show the detection of rHbII at different temperature of induction. The lanes 2-3 show the rHbII detection when the induction temperature was 25°C; lanes 4-5 when the induction temperature was 30°C and lanes 6-7 when the induction temperature was 37°C. 37

3.4 Sodium dodecyl sulfate polyacrylamide gel electrophoresis (SDS-PAGE) analysis for the detection of rHbII when different *E. coli* strains were used. Lane 1 contains the SDS-PAGE standard and the lanes 2-5 show the rHbII samples. The lanes 2-3 show the rHbII detection when the BL21 *E. coli* strain was used 39

and lanes 4-5 when the BLi5 *E. coli* strain was used.

3.5 A sigmoid bacterial growth curve of the rHbII expressed in BLi5 *E. coli* cells. The bacterial growth is represented by a curve that consists of three phases: lag phase, log phase and stationary phase and each points of the curve is a measure of the optical density in a 30 minute interval. 41

3.6 Sodium dodecyl sulfate polyacrylamide gel electrophoresis (SDS-PAGE) analysis of each step of the recombinant HbII purification. The purification process was performed using metal affinity chromatography with a cobalt resin. Lanes 1 and 8 contains the SDS-PAGE broad range molecular weight standard and the lanes 2-7 show each step of purification. Lane 2 contains the crude lysate; lane 3 contains sample of the pass through steps; lane 4 contains sample of the wash step; lane 5 contains sample of the elution steps before appearance of the HbII band and lanes 6 and 7 contain rHbII after purification. 43

3.7 UV-Vis spectra of the oxy rHbII obtained after TALON Purification. The spectrum shows a Soret band at 414 nm and Q bands at 540 and 576 nm identical to wild type HbII-O_2 indicating that the heme group was incorporated during the expression process. 44

3.8 UV-Vis spectra of the formation of the deoxy rHbII complex obtained after TALON purification. The spectrum shows a Soret band at 432 nm and Q bands at 556 nm identical to wild type HbII. To obtain this spectra, the rHbII sample was treated with sodium dithionite. 45

3.9 UV-Vis spectra of the formation of the rHbII-CO complex obtained after TALON Purification. The spectrum shows a Soret band at 420 nm and Q bands at 539 and 570 nm identical to wild type HbII-CO. To obtained this spectra the rHbII sample was treated with sodium dithionite and exposed to a CO atmosphere. 47

3.10 UV-Vis spectra of the Soret bands for the carbon monoxide (—), deoxy (—) and oxy (—) rHbII complex. 48

3.11 UV-Vis spectra of the Q bands for the carbon monoxide (—), deoxy (—) and oxy (—) rHbII complex. 49

3.12 UV-Vis spectra of the formation of the met-acid rHbII complex. The complex formation was monitored at different pH: 6.5 (- -), 5.0 (…),and 4.0 (—). Spectra measurements were made after 2 51

minutes of the 0.1 M HCl addition.

3.13 UV-Vis spectra of the formation of the met-hydroxide rHbII complex. The complex formation was monitored at different pH: 7.5 (- - -), 9.5 (- -), and 11.0 (—). Spectra measurements were made after 2 minutes of the 0.1 M HCl addition. 52

3.14 UV-Vis spectra of the Q bands for the formation of the met-hydroxide rHbII complex. The complex formation was monitored at different pH: 4.0 (--), 7.5 (- -), 8.5 (--), 10.5 (---) and 11.0 (—). Spectra measurements were made after 2 min of the 0.1 M NaOH addition. 53

3.15 Kinetic trace for the O_2 association of the recombinant HbII. The kinetic was followed at 414 nm in a stopped-flow apparatus. All these data were collected for 0.3 seconds at a rate of 1000 scans/sec. 55

3.16 Plot of the negative of the absorbance values against time for rHbII. The negative of the absorbance values are used to make the exponential fit of the kinetic model. 56

3.17 Plot of the negative of the absorbance values against time for rHbII at a concentration of 325 μM of an oxygen solution. The red dot represents a residual plot for the experimental data set. The red line represents the exponential decay analysis which is described by the following equation, $y = 0.4421\ e^{(-83.06x)} - 1.111$ `57

3.18 Plot of the negative of the absorbance values against time for rHbII at a concentration of 141 μM of an oxygen solution. The red dot represents a residual plot for the experimental data set. The red line represents the exponential decay analysis which is described by the following equation, $y = 0.3025\ e^{(-53.50x)} - 1.080$ 58

3.19 Plot of the negative of the absorbance values against time for rHbII at a concentration of 61 μM of an oxygen solution. The red dot represents a residual plot for the experimental data set. The red line represents the exponential decay analysis which is described by the following equation, $y = 0.1465\ e^{(-30.40x)} - 0.974$ 59

3.120 Plot of the negative of the absorbance values against time for rHbII at a concentration of 23 μM of an oxygen solution. The red dot represents a residual plot for the experimental data set. The red line represents the exponential decay analysis which is described by the following equation, $y = 0.1205\ e^{(-29.67x)} - 0.9172$ 60

3.21 Plot of the negative of the absorbance values against time for rHbII at a concentration of 10 μM of an oxygen solution. The red dot represents a residual plot for the experimental data set. The red line represents the exponential decay analysis which is described by the following equation, $y = 0.1738\ e^{(-20.82x)} - 0.9547$ 61

3.22 Plot of k' versus $[O_2]$ concentration for the wtHbII and the rHbII. The k_{on} was obtained from the slope of the line. 63

3.23 Kinetic trace for the O_2 dissociation from the recombinant HbII (..) and the wild type HbII (◊). The red line (---) represents the first order exponential decay analysis for each kinetic. A solution of 3 mg/mL of sodium dithionite was used to reduce the Fe and obtain the oxygen dissociation. The time courses of the kinetic were monitored at 414 nm in a UV-Vis spectrophotometer. 65

3.24 Kinetic trace for the autoxidation of the recombinant HbII. The red line (---) represents the first order exponential decay analysis for the kinetic. The time courses of the kinetic were monitored at 414 nm in a UV-Vis spectrophotometer. 67

Introduction

1.1 Hemoglobin

In the last decades, scientists around the world tried to improve oxygen transport and greater heme stability. In this regard, they concentrated their efforts on understanding the structure, function, and ligand binding of different hemoglobins (Hbs). To achieve this goal they used protein engineering to reconstruct the heme pocket stereochemistry and to elucidate the different functions of hemoglobins. Hemoglobins have been discovered in organisms from all kingdoms, nevertheless their function is not the same among them. Bacteria, protozoa, fungi and invertebrates have hemoglobins, but the roles of these hemoglobins include the reversible binding of gaseous ligands such oxygen (O_2), nitric oxide (NO), carbon monoxide (CO), cyanide (CN^-), and hydrogen sulfide (H_2S) (Egawa el. al., 2005). The hemoglobins in bacteria are known as flavohemoglobins and they are NO dioxygenases for detoxifying NO (Ouellet, et al., 2007). In protozoa and plants, hemoglobins are largely involved with electron transfer and O_2 storage and scavenging (Schechter, 2008). A variety of mechanisms for oxygen transport and binding proteins exits in organisms throughout the animal and plant kingdoms.

Human hemoglobin is a globular metalloprotein and consists of four globular protein subunits, two α and two β globins (Figure 1.1A). Each protein chain is arranged into a set of alpha-helix structural segments connected in a globin fold arrangement (Figure 1.1B). The hydrogen-bonding interaction in hemoglobin occurs between the H of an $^-$NH groups and the O of $^-$CO groups of the polypeptide backbone chain. The protein chain in the hemoglobin is tightly associated with a non-protein heme group by noncovalent forces (Schechter, 2008). A heme group consists of an iron ion held in a heterocyclic ring, known as protoporphyrin IX (Figure 1.2A).

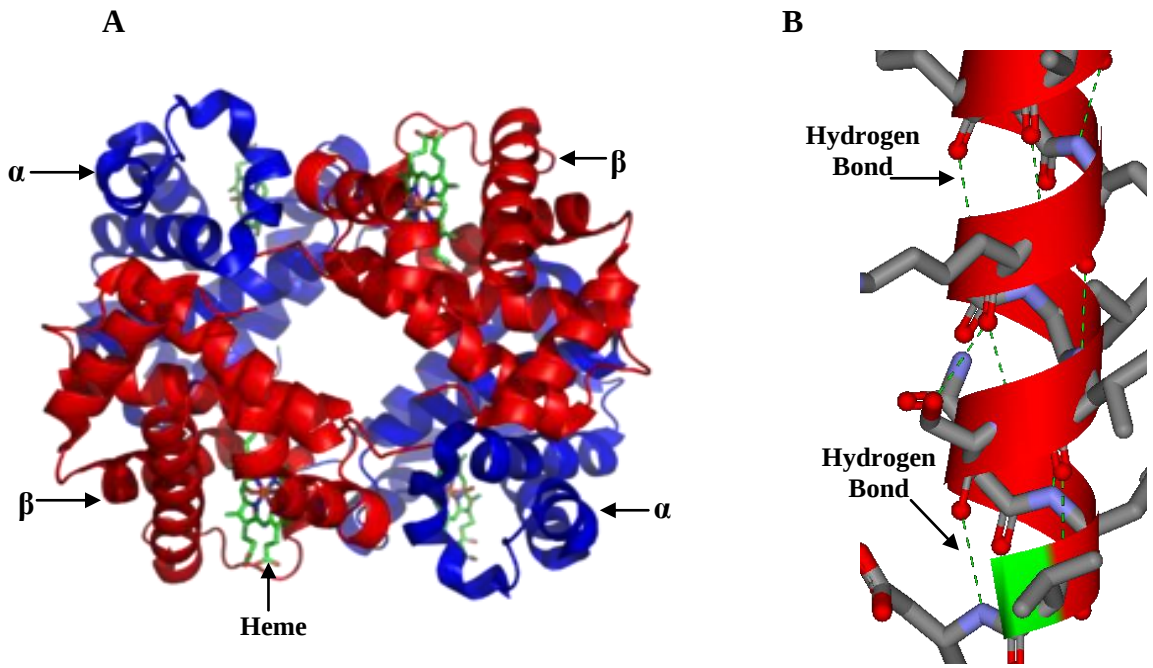

Figure 1.1 Quaternary structure of hemoglobin (A). The hemoglobin consists of two α (blue) and two β (red) chains, each one attach to a heme prosthetic group (green). Each alpha-helix structure (B) is hydrogen-bonded to the amino acid between the –NH and –CO functional groups. Taken from: PDB: 1GZX; PDB: 1FLP

The iron ion in the protoporphyrin is primarily in the physiologic ferrous (Fe^{II}) chemical valence state when it binds with oxygen. The iron atom is the site of oxygen binding and is coordinated to 4 pyrrole nitrogen atoms in the center of the ring, which all lie in one plane. It is also bound strongly to the globular protein via the imidazole ring of the F8 histidine residue located below the porphyrin ring (Figure 1.2B). The sixth position in the heme group can reversibly bind oxygen or other gas atoms on the side opposite the histidine residue, completing the octahedral group of six ligands (Schechter, 2008). Two different hemoglobin structures were identified depending on wheter an atom is attached or not to the sixth position. These structures are the T (tense) and the R (relaxed) state associated with the deoxygenated and the oxygenated form of the protein, respectively (Mozzarella, 2008). In the oxygenated state (R) of the hemoglobin, a molecule of oxygen is attached to the Fe. The porphyrin ring adopts a planar configuration and the Fe^{II} lies in the plane of the porphyrin ring (Figure 1.3A). When oxygen is not bound, (deoxygenated state, T), the heme group is in a nonplanar geometry (Figure 1.3B). As a consequence, the iron atom is pulled out of the plane of the porphyrin toward the histidine residue to which it is attached.

1.2 Blood substitutes

In the last years, America's blood deficiency has propelled the biotechnology of blood substitutes. Hemoglobin-based oxygen carriers (HBOCs) also known as “blood substitutes” have been under active clinical development over the last two decades (Alayash, 2008). In addition, their ability to work with the same efficiency as hemoglobin has been studied by many research groups during recent years. The use of synthetic blood may be the solution to a predicted deficit of packed red blood cells that will be required because of an aging population, increased blood use and decreased allogeneic collection (Mackenzie, 2005).

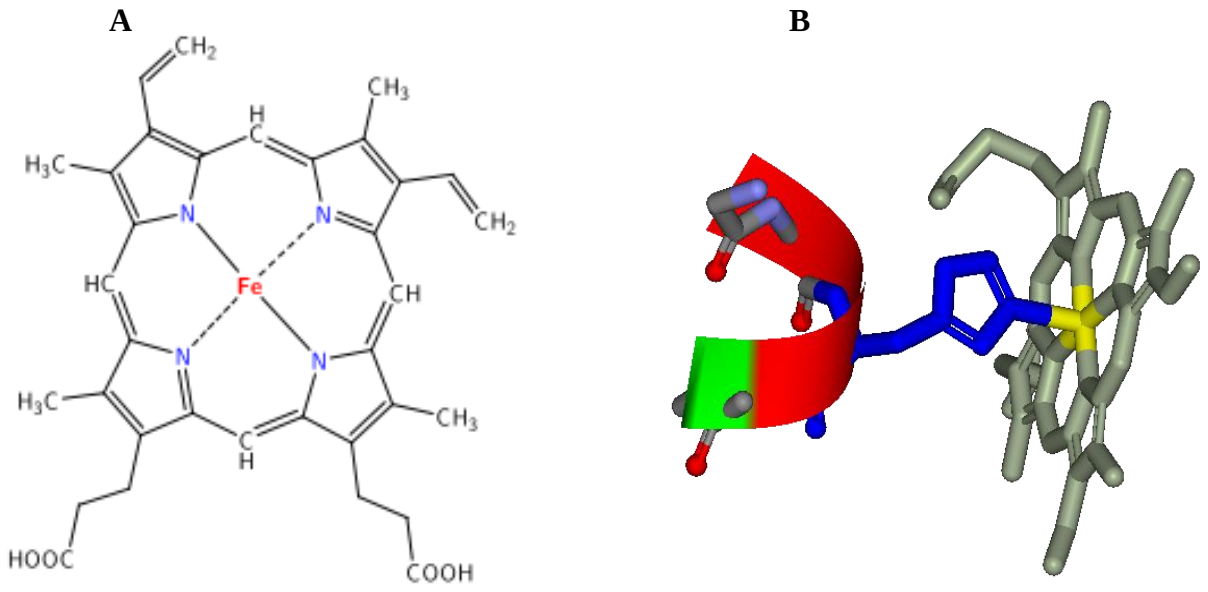

Figure 1.2 Schematic representation of the heme group (A) which contains a Fe iron in the center attached to four nitrogens of a heterocyclic macromolecule called a porphyrin. The heme group is attached to the globin by the histidine residue in the F8 helix (B). Taken from: PDB: 1FLP

A **B**

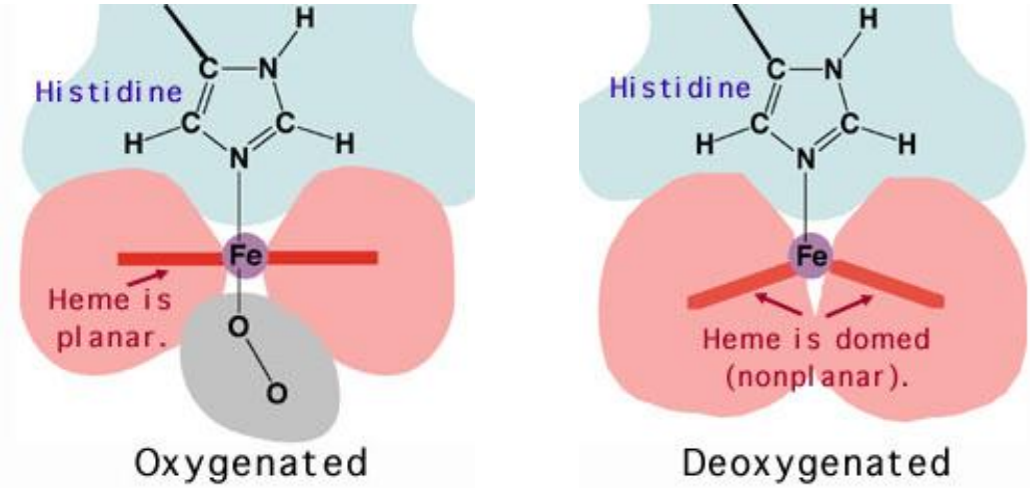

Figure 1.3 Schematic diagram of the planar configuration adopted by the porphyrin ring in which in the oxygenated state (A) the heme group is planar and the Fe has a charge of Fe^{II}. In the deoxygenated state (B) the heme group is nonplanar and the iron has a charge of Fe^{III}.

As a result of an increased demand, during the last years, the efforts to produce a blood substitute are increasing because of two security issues. One of these facts, is the need of safe alternatives for blood transfusions to avoid the risk of infection with HIV and other blood borne pathogens (Alayash, 2004; Herol et al., 2003; Burmester et al., 2000). The other is the possible lack of supplies after a serious accident or in cases of anemia. To avoid transfusions for acute blood loss in trauma, or when blood is unavailable or refused, oxygen-carrying solutions could be used as a new alternative. Furthermore, blood substitutes are a new option for individuals who are immunoreactive to every blood type and pre-term infants who, when exposed to repetitive adult blood transfusions, develop chronic pathologies such as bronchopulmonary dysplasia and retinopathy of prematurity (Mozzarelli, 2008). Blood substitutes could also be used by those who practice their religion as Jehovah Witnesses, who refuse transfusions (Everts, 2009; Mozzarelli, 2008). Artificial blood does not contain the plasma, red and white cells, or platelets of human blood, but it can perform the functions to transport and deliver oxygen to the body's tissues until the recipient's bone marrow has regenerated the missing red blood cells (Squires, 2002).

To be a good oxygen carrier is not the only characteristic that is needed in a blood substitute; it also needs to have an adequate oxygen affinity to oxygenate tissues without the production of oxygen radicals, have antioxidant properties and low autoxidation rates, and low reaction with nitric oxide (Dimino et al., 2007; Jia et al., 2004). Like most technological advances, there are still a number of advantages and disadvantages to consider with blood substitutes. For example, in addition to carrying oxygen, the compounds of a blood substitute need to be sterilized against infectious diseases to be used in patients whose religious beliefs prevent them from accepting blood transfusions. Another advantage is that the blood substitutes present is that they allow for immediating full-capacity oxygen transport, as opposed to transfused blood which can require about 24 hours to reach full oxygen transport capacity due to

2,3-diphosphoglycerate depletion. Also their long shelf life and the ability to be stored at room temperature are other advantages of blood substitutes compared to donor blood which has only a 28-day shelf life and requires cold storage (Tinmouth et al., 2008; Winslow, 2008; Spahn et al., 2005). Currently, the hemoglobin–based oxygen carriers present side effects such as adverse cardiac events, tissue damage, coagulation changes, renal toxic effects and adverse effects on vascular tone and blood pressure (Baldwin el. al., 2004). Other disadvantages that blood substitutes present are their relatively short half-life after administration (24-48 hours) and their interference with laboratory hemoglobin measurements (Tinmouth et al., 2008).

At present, the main focus is to find or develop a blood substitute to mimic the ability of red blood cells to bind oxygen in the lungs, release it, and eliminate the potential toxicity of hemoglobin when it is outside a red blood cell (Everts, 2009). Scientists have developed chemical modifications to prevent the breakdown of cell free Hb. Table 1.1 shows the main options that exist for modifying Hb: conjugation; cross-linking; polymerization and encapsulation. Also hemoglobin-based oxygen-carrier products are made of modified stroma-free Hb from human, animal or recombinant origin (Becker, 2001). The conjugated hemoglobin was produced by increasing the molecular weight of Hb, by bonding it with a water-soluble polymer (Goorha et al., 2003). The compound diaspirin (3,5-dibromosalicyl fumarate) was used to cross-link, α-units and, β-units of Hb in the cross-linking modification. Furthermore, for recombinant Hb (rHb), few parts of an amino acid sequence of human Hb are replaced to prevent the dissociation into dimers and to maintain adequate oxygen affinity.

Table 1.1: Different types of blood substitutes and the hemoglobin structural modifications to maintain the tetramer structure.

Modification	Description	Representation
Conjugation	The surface of hemoglobin is decorated by adding molecules such as polyethylene glycol (PEG). This alters the oxygen binding properties of the hemoglobin and helps prevent it from damaging the kidney.	
Cross-linking	Chemical modifications join the components of hemoglobin together, preventing it from falling apart.	
Polymerization	Chemical cross-links are created between different hemoglobin molecules, holding them together and preventing them from falling apart.	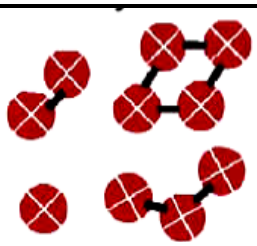
Encapsulation	Hemoglobin molecules are enclosed within a lipid membrane, which can contain high concentrations of hemoglobin, which discourages it from falling apart.	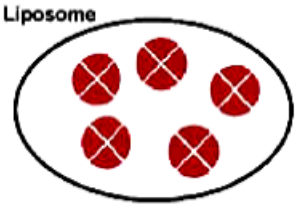
Recombinant hemoglobin	Few parts of an amino acids sequence of human Hb are replaced to prevent the dissociation into dimers and to maintain adequate oxygen affinity.	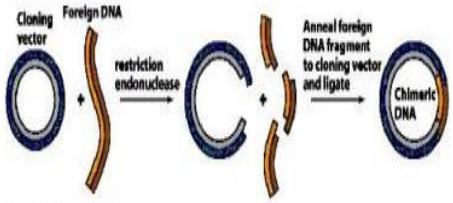

Alayash, 1999; Goorha et al., 2003 and Chang, 2003.

Currently, more than 50,000 blood substitutes' patents have been filed and some have reached Phase III in clinical trials (Events, 2009). Table 1.2 shows some of these HBOCs that are under clinical trials and their adverse effects (Tinmouth et al., 2008). HemAssist from Baxter Healthcare was the first hemoglobin-based oxygen carrier that goes to clinical trials (Events, 2009; Rabinovici, 2001). A Phase III trauma trial in the U.S. was stopped after nearly half of the patients died after they received this hemoglobin. The diaspirin cross-linked Hb (α-DBBF Hb) is another of these products under study; it is an intramolecularly cross-linked tetramer produced via chemical reaction with bis(3,5- dibromosalicyl) fumarate. Clinical studies with α-DBBF Hb showed that initially, it reduced the need of blood transfusion in cardiac and noncardiac surgery patients. Nevertheless its administration was stopped after an analysis indicated higher mortality in the treatment group than in the control group and it has been removed from the market (Tinmouth el. al., 2008). Other hemoglobin substitutes under investigation involve the polymerization of blood cells, PolyHeme, which is derived from outdated human blood and Hemopure, derived from bovine hemoglobin. Initially, the Food and Drug Administration (FDA) approved to run a human trial with PolyHeme in trauma patients but after critical media reports about bioethicists and patients rights groups, several hospitals pulled out of the trials. But in 2007, Northfield Laboratories published results about clinical trials with PolyHeme and requested that the FDA to approve it. They are waiting for an answer from the FDA (Events, 2009). Hemopure was associated with a reduction in the need for blood transfusion in patients undergoing elective orthopedic, cardiac, and noncardiac surgery (Tinmouth el. al., 2008). It was approved in South Africa but studies made by the FDA demonstrated that it shows vasoconstrictive adverse effects.

Table 1.2: Different types of blood substitutes and their adverse effects

Hemoglobin-based carriers products	Chemical modifications	Adverse effects
HemAssist, Baxter Healthcare Corporation	Cross-linking	• Hypertension • Severe vasoconstriction complications • Higher mortality in treatment group tan in the control group
Hemopure, Biopure Corp.	Pyridoxylation	• Vasoconstrictive effect.
Hemolink, Hemosol BioPharma	Polymerization	• Severe abdominal pain • Increase in mean arterial pressure
α-DBBF Hb	Cross-linking	• Relative short half-life after administration

Everts, 2009; Natanson, et. al, 2008; Tinmouth et al., 2008

The conjugated human Hb (Hemospan) is another HBOCs under clinical trial, which is construct with up to eight polyethylene glycol (PEG) molecules. Hemospan can facilitate the transfer of oxygen from red blood cells to tissue where tissue PO_2 is low and the release of O_2 in resistance vessels by it is restricted and vasoconstriction is greatly reduced (Winslow, 2008). It may be administered to patients in shock because, in addition to its ability to oxygenate tissue, it is a powerful blood volume expander. Other HBOCs is Optro, which is a cross-linked Hb from genetically modified *E. coli* bacteria and is the only recombinant hemoglobin in clinical trial. It is another HBOCs that was tested in clinical trials and its advantage is that genetic control theoretically can be used to improve the current product source to eliminate problems such as unwanted vasoconstriction (Rabinovici, 2001). Also, the invertebrate hemoglobins have shown to be a potential alternative as hemoglobin-based oxygen carriers. For example, European researchers are producing a blood substitute using the *Lumbricus terrestris*, commonly known as the earth-worm, and the *Arenicola marina*, a marine worm (Rousselot et al., 2006; Hemarina, 2008).

Furthermore, previous studies demonstrated that the cell free-hemoglobins are toxic substances that can autoxidize and generate reactive oxygen species (ROS), or can be oxidized by their interaction of the ROS. ROS can be nitric oxide (NO), hydrogen peroxide (H_2O_2), peroxynitrite ($ONOO^-$) and the hydroxyl radical ($OH^{\cdot}$). Nevertheless the oxidative reactions significantly affect the stability of the cell-free hemoglobins (Yeh et al., 2003).

The new generations of HBOCs have been modified to prevent rapid dissociation and short half-life, to avoid renal toxic effects, and to reduce vasoconstriction by decreased NO scavenging. For these reason, studies including the modifications in the heme pocket amino acids, are focused to identify the mechanism of oxygen carriers to reduce the reactivity of the hemoglobin with oxidants and with NO.

It is important to understand the role of heme pocket chemistry in determining these reactions. The studies of the diversity of invertebrate hemoglobins at the structural and functional levels provide a new route to investigate ligand binding to these proteins. In particular, the hemoglobins of the clam *Lucina pectinata* are a good model for these studies.

1.3 Hemoglobin II of Lucina pectinata

L. pectinata is a bivalve mollusk that inhabits the sulfide rich sediments of the west coasts of Puerto Rico and it houses chemoautotrophic bacteria in which three hemoglobins deliver and transport oxygen and hydrogen sulfide. The hemoglobin I (HbI) is a monomeric sulfide-reactive protein of 142 amino acids which reacts with hydrogen sulfide (H_2S) to form ferric hemoglobin sulfide. In contrast, the hemoglobin II (HbII) and hemoglobin III (HbIII) are oxygen-reactive proteins that remain oxygenated in the presence of hydrogen sulfide (Kraus and Wittenberg, 1990).

Hemoglobin II is a dimeric hemoglobin of 151 amino acid residues with a full-length cDNA sequence of 2114 nt (Torres et al., 2003). Studies made by Kraus and Wittenberg demonstrated that the hemoglobin II is a monomer at low concentrations, while at high concentrations HbII form aggregates. Recently, the HbII crystal structure (Figure 1.4) was resolved showing to be a dimer at concentration ~ 1-2 mM, (Gavira et al., 2006; Gavira et al., 2008). Similar to the other hemoglobins of *L. pectinata,* HbII has a glutamine (GlnE7) in the distal position of the heme pocket instead of a histidine. In addition, these Hb's have phenylalanine in the E11 and CD1 positions; but in the B10 position, HbII has a tyrosine (Figure 1.5A). In HbII, the oxygen is tightly anchored to the heme through hydrogen bonds with TyrB10 and GlnE7 (Figure 1.5B).

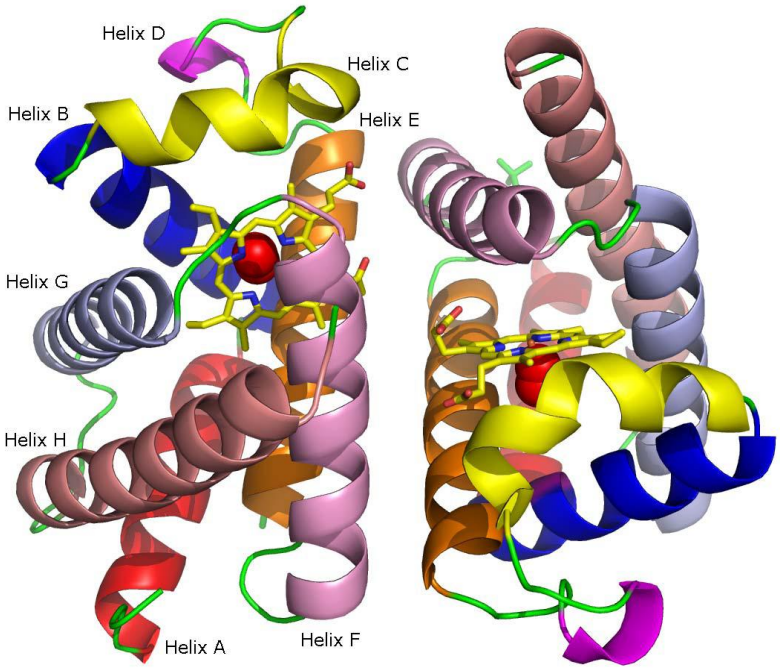

Figure 1.4 X-ray structure of Hemoglobin II of *Lucina pectinata*. HbII is an oxygen binding hemoglobin and consists of two dimers of 163 amino acids. Each globin consist of six α-helices surrounding the central heme pocket, and two minor helical segments between the B and E helices (Gavira et al., 2008)

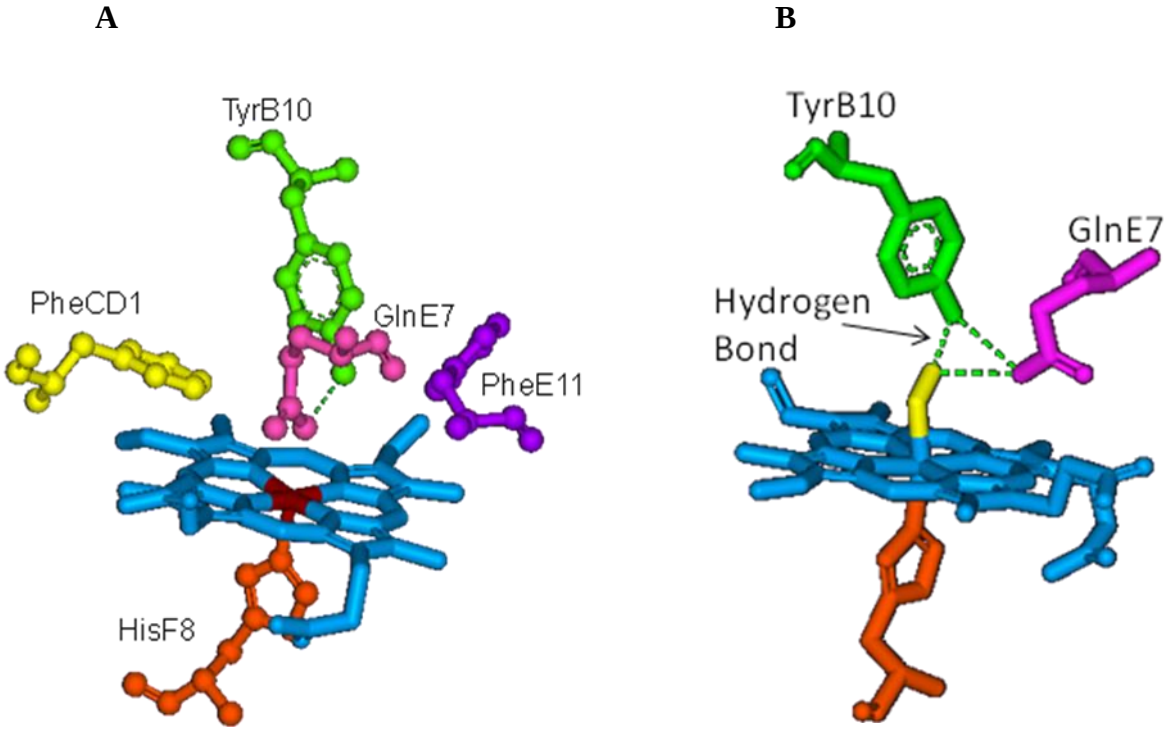

Figure 1.5 Diagram of the orientations of the distal residues of the wild type HbII from *L. pectinata* (A). In the distal site of the heme pocket HbII is GlnE7 instead of the classical histidine. The other surrounding amino acid residues are PheCD1, PheE11 and TyrB10. In the hydrogen bond network of HbII, the oxygen is tightly anchored to the heme through hydrogen bonds with TyrB10 and GlnE7 (B). Taken from: PDB: 2OLP

The proximal HisF8 is hydrogen bonded to a water molecule, which interacts electrostatically with a propionate group, resulting in a Fe-His vibration at 211 cm^{-1} (Gavira et al., 2008). The combined effects of the HbII small heme pocket, the hydrogen bonding network, the His trans-effect, and the orientation of the oxygen molecule confer stability to the oxy-HbII complex. Oxidation of HbII only occurs when the pH is decreased from pH 7.5 to 5.0. Structural and Resonance Raman Spectroscopy studies suggest that HbII oxygen binding and transport to the host bacteria may be regulated by the dynamic displacement of the GlnE7 and TyrB10 pair toward the heme to protect it from changes in the heme oxidation state from Fe^{II} to Fe^{III}.

The oxygen affinities for HbII is the same of HbI and HbIII (P_{50} = 0.1-0.2 torr) and are independent of pH. The association (k_{on}) and dissociation (k_{off}) of HbII with O_2 are slow compared with HbI ($k_{on} = 0.390 \times 10^{-6}\ M^{-1}s^{-1}$ and $k_{off} = 0.11\ s^{-1}$) (Kraus and Wittenberg, 1990). This slow oxygen off rate and the stabilization of the oxygenated structure of HbII is mostly a consequence of a strong hydrogen bond network between the GlnE7, TyrB10 and the bound ligand, which precludes transport or diffusion of O_2 as a major function (Pietri et al., 2005).

Studies made by De Jesús-Bonilla and co-workers showed that HbII is resistant to hydrogen peroxide oxidation due to the Tyr in the B10 position (De Jesus-Bonilla et. al, 2006). The tyrosine creates a hydrogen networking that stabilizes the radical form of the compound II ferryl species. Experiments performed with the wt-HbII showed reduced bands, suggesting that the TyrB10 orientation and the volume of the heme pocket play a distinctive role in the ferryl formation of the hemeproteins (De Jesus-Bonilla et. al, 2006). At an acidic pH (5.0), the tyrosine OH is assumed to be protonated and water ligates to the ferric heme. Meanwhile, at an alkaline pH (11.2), the tyrosyl competes with hydroxyl radical as a ligand to the heme iron (Pietri et al., 2005).

These results can be explained by changes in the heme coordination and ligation state during titration of HbII. Other studies performed by De Jesús-Bonilla and co-workers showed that HbII exhibited the fastest NO dissociation rate ($k_{off,NO}$ = 7.1 x 10^{-4} s^{-1}) and the slowest NO association with ferrous iron (De Jesus-Bonilla et. al, 2007). The autoxidation, H_2O_2-mediated ferryl iron (Fe^{IV}) formation, and the subsequent heme degradation kinetics were much slower in HbII when compared to those of HbI (De Jesus-Bonilla et. al, 2007). The TyrB10 residue in HbII appears to afford a greater heme oxidative stability advantage toward H_2O_2, whereas the close proximity of this residue together with GlnE7 to the heme iron contributes largely to the distal control of NO binding. As a result, of the role of HbII in the NO physiology of the clam *Lucina pectinata*, the unusually well controlled NO entry in heme pocket, and based on the kinetic and structural data of HbII, it may represent a model for the design of future oxidatively stable oxygen therapeutics with little or no vasoactivity. Is for this reason, that we are focused using the recombinant hemoglobin II to determine and understand the mechanisms that may improve the production of blood substitute prototypes.

1.4 Objectives

The expression of recombinant Hemoglobin II (rHbII) in *Escherichia coli* and the pET28 plasmid in a fermentor was the main goal of this project. After expression, the rHbII was purified by affinity chromatography using a metal affinity resin. To characterize the protein, different complexes were formed with diverse ligands. Also, the oxygen association and dissociation of rHbII were determined using a stopped flow system to perform the measurements of the kinetics in a millisecond time scale.

MATERIALS AND METHODS

2.1 Construction of rHbII into pET28 (a+) vector

To generate a representative sample of recombinant HbII (rHbII) protein, it was necessary to perform subsequent molecular and biophysical studies of their respective ligand binding and allosteric properties. Site directed mutagenesis of HbII is necessary to improve oxygen binding and induce allosteric properties. To obtain the rHbII sample needed, it was necessary to follow the procedures of cloning, protein expression, protein lysis, and protein purification. The construction of the rHbII was done according to the procedure found in the literature (R.G. Leon et al., 2004). Aliquots of 2 mL of the vector were provided to our laboratory by Dr. Cadilla from the UPR-Medical Science Campus. The *Hind III* and the *XhoI* restriction sites of the vector's polylinker region were used to clone the HbII cDNA inserts into the pET-28a(+) vector. (Fig 2.1)

2.2 Preparation of BLi5 and BL21 competent cells

A 100 mL culture of BLi5 cells with 100 µL chloramphenicol (30 µg/mL) and 100 µL kanamycin (70 µg/mL) was grown in LB medium (98% H_2O, 1% Tryptone, 0.5% Sodium Chloride, and 0.5% Yeast extract) at 250 rpm and 37°C. The culture was allowed to reach to an OD_{600} between 0.5 and 1. The culture was transferred aseptically to the 50 mL Falcon tubes. A 0.1M $CaCl_2$ solution was cooled on ice for ten minutes. The cell culture was centrifuged at 4°C and 4,000 rpm, for 10 minutes. The supernatant was decanted and the bacterial pellet was resuspended in 50 mL of 0.1M $CaCl_2$ and centrifuged again as before. The supernatant was decanted and this second pellet was resuspended in 25 mL of 0.1M $CaCl_2$. The suspension was centrifuged again as before and the supernatant was decanted.

pET-28a Vector

pET-28a(+) sequence landmarks	
T7 promoter	370-386
T7 transcription start	369
His• Tag coding sequence	270-287
T7• Tag coding sequence	207-239
Multiple cloning sites (*Bam*H I - *Xho* I)	158-203
His• Tag coding sequence	140-157
T7 terminator	26-72
lacI coding sequence	773-1852
pBR322 origin	3286
Kan coding sequence	3995-4807
f1 origin	4903-5358

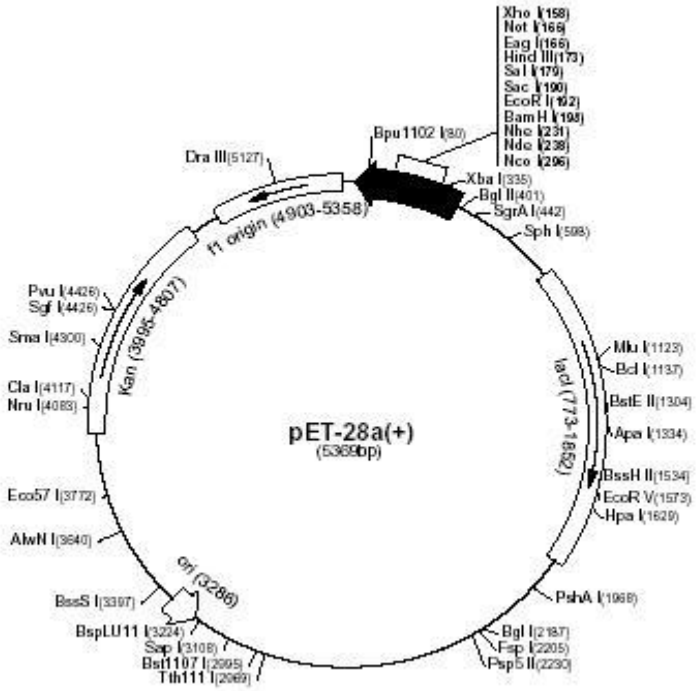

Figure 2.1 Diagram of the pET-28a(+) expression vector which contains a T7 promoter, 6X-His tags and a LacI gene. This plasmid confers resistance to kanamycin and has a polylinker region that may be used for directional cloning. This illustration was taken from www.pasteur.ac.ir

The resulting bacterial pellet was resuspended in 2 mL of a 10% glycerol solution. The suspension was again centrifuged as described. Finally, the competent cells were used for the thermal-shock or otherwise stored at -80 °C to enhance their life period. A similar procedure was performed with the BL21 cells, with the exception that the culture was grown in 100 μL kanamycin with a concentration of 70 μg/mL.

2.3 *Transformation of pET28(a+) vector in the BLi5 cells*

For the bacterial transformation, a pET-28a(+) plasmid that contained the HbII cDNA sequence was introduced in the BLi5 or BL21 cells by chemical transformation (Leon et al., 2004). Two microliters of DNA plasmid were mixed with 250 μL of competent cells and placed on ice for 30 min. The cells were heated without agitation for 45 sec at 42 °C in a water bath. Immediately, the tubes were placed on ice for at least two minutes. Then 800 μL of SOC medium (2% w/v bacto-tryptone, 0.5% w/v bacto-yeast extract, 8.56mM NaCl, 2.5mM KCl (0.186g), 10mM $MgCl_2$ and 20mM glucose) at room temperature were added to each tube and placed in a water bath at 37 °C and 120 rpm for 45 minutes. The bacterial suspensions were placed on agar plates containing selective antibiotics and incubated overnight at 37 °C. Recombinant colonies expressed in BLi5 cells were selected in a media containing kanamycin (70 μg/mL) and chloramphenicol (30 μg/mL). Recombinant HbII expressed in BL21 cells were selected in kanamycin media. Plasmid minipreps purifications were performed using a QIAprep Spin Miniprep Kit from Qiagen for the selected colonies grown in 5 mL of Luria broth (LB) broth and the corresponding antibiotics. Aliquots of 1 μL of plasmid DNAs were mixed with the restriction enzymes and incubated at 37°C for 3 hr. The *XhoI and HindIII* enzymes were used to verify inserts of constructs prepared in the pET28 vector. Subsequently, an electrophoresis analysis of 1% agarose gels in 1X TBE was done to verify if the inserted cDNAs were present.

The electrophoresis gel was run at 100V for one hour. To enhance the life of the recombinant colonies, 10% sterilized glycerol was added and the colonies were stored at a low temperature (-80 ºC).

2.4 Pilot Expression

For the pilot expression, 100 mL of an overnight culture were inoculated in 900 mL of fresh Terrific broth medium (TB) with the corresponding antibiotics in Fernbach flasks. The new culture was grown at 37°C and 125 rpm to reach an OD_{600} between 1.5 and 2.0. At that point, the culture was induced with 1 mM IPTG and supplemented with 1% w/v glucose and 30 μg/mL hemin chloride. Different experimental conditions were analyzed to obtain a better yield. The type of *E. coli* strains (BL21 or BLi5) were the first variable tested. Both strains were induced during the log phase with 1 mM IPTG. Also, the media was supplemented with 30 μg/mL hemin chloride and 1% w/v of glucose, and the temperature was decreased to 30°C. Different temperatures after induction were analyzed following the procedure described for the induction in the log phase. The cultures were grown at 37 °C, but when it was induced the temperature was changed to 25, 30, or 37 °C. The induction time was also analyzed. The induction with 1 mM IPTG was performed both in the lag phase (OD_{600} between 1.0-1.4) and log phase (OD_{600} between 1.5-2.0). All these parameters were analyzed to determine the optimum conditions that increase the amount of protein produced by the bacteria.

2.5 High-level Expression of rHbII in E. coli

High-level protein expression was done using a BioFlo 110 Modular Benchtop fermentator as described in the literature (Leon et al., 2004). The expression procedure required at least two days of pre-work to obtain a better protein yield. The necessary solutions were prepared to perform the expression procedure: 500 mL of Luria broth medium (98% H_2O, 1% Tryptone,

0.5% Sodium Chloride, and 0.5% Yeast extract), 250 mL of 50% w/v glucose, 500 mL of 1.5 M monobasic potassium phosphate (KH_2PO_4,), 500 mL of 30% v/v ammonium hydroxide (NH_4OH,), 5 mL of 1 mM IPTG and 500 mL containing 0.17 M KH_2PO_4 and 0.72 M K_2HPO_4. All the solutions were sterilized for 20 min at 120 ºC, with the exception of the 30% v/v NH_4OH and the IPTG solution. Two days before the fermentation, transformed cells were grown in 50 mL of LB medium and the corresponding antibiotics (30 μg/mL of chloramphenicol and 70 μg/mL of kanamycin). The cells were placed overnight in a shaker at 120 rpm and 37 °C. After this period, the culture was transferred to a 250 mL sterilized Erlenmeyer with 50 mL of Luria broth medium and incubated for 12 hours in a shaker incubator at 120 rpm and 37 °C. Then, the culture was transferred to a 2500 mL flask adding 500 mL of the LB medium. The culture was incubated overnight in a shaker incubator at 37°C and 120-150 rpm. The day before the expression, 4.0 L of the TB medium (48 g Tryptone, 96 g Yeast Extract, 16 mL glycerol and 3,600 mL of H_2O) were prepared in a fermentation vessel. The water jacket of the vessel was filled and the vessel was sealed. Then, the vessel was placed in a Sanyo autoclave and sterilized at 121 ºC for 60 min.

For the expression process, the cells were grown in a BioFlo 110 Modular Benchtop (Figure 2.2). The sterilized vessel containing the TB broth was removed from the autoclave and placed in the stirring base. The hoses and temperature probe were connected to lower the temperature of the media to 37 ºC. Once this temperature was reached, the corresponding antibiotics were added: 30 μg/mL of chloramphenicol and 70 μg/mL of kanamycin. To prevent an excess foaming 500 μL of antifoam solution and the sterile solution of 0.17M KH_2PO_4 and 0.72M K_2HPO_4, which contain 2.52 g of magnesium sulfate, were added to the broth.

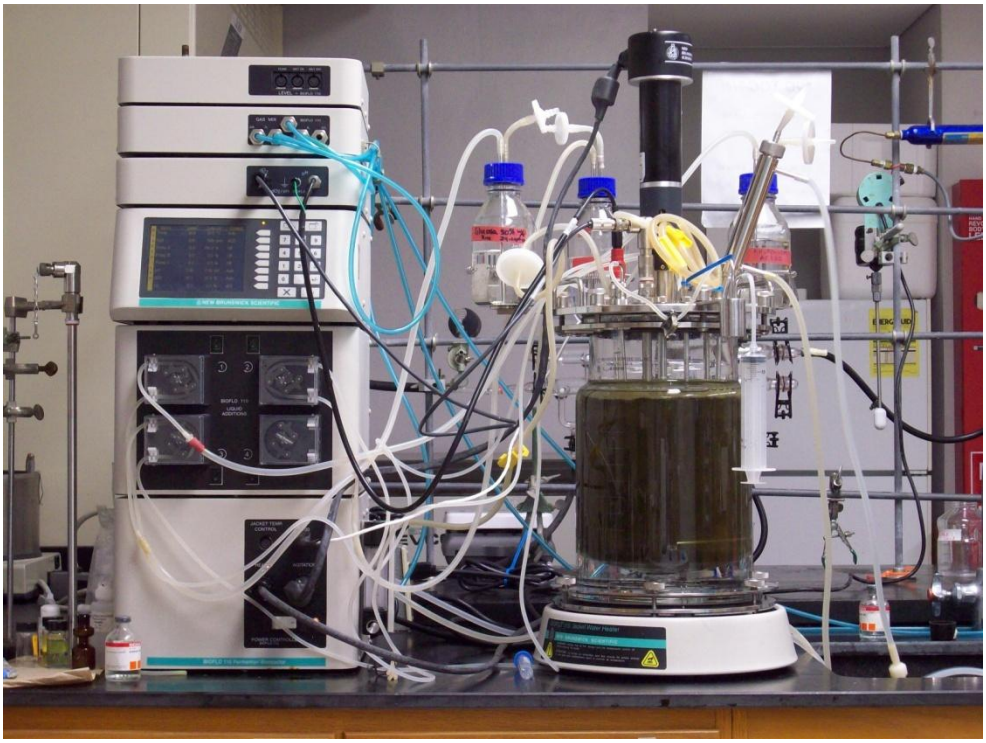

Figure 2.2 BioFlo 110 Modular Benchtop Fermentator of New Brunswick used to grow the BLi5 cells that produced the recombinant Hemoglobin II from *Lucina pectinata.* The Bioreactor includes a Primary Control Unit (PCU) and Power Controller to manage temperature, agitation, pH and pO_2.

The pH sensor was calibrated to a pH of 7.0 and introduced inside the vessel. The dissolved oxygen (dO_2) sensor was introduced and calibrated inside the vessel to a dO_2 of 35%. A measurement of optical density at 600 nm (OD_{600}) in a UV-Vis scanning spectrophotometer was taken as reference to monitor the cell growth along the expression procedure. The overnight culture was inoculated in the 4.5 L TB media and the OD_{600} was taken. The OD_{600} was measured every 30 minutes to monitor the cell growth. The protein expression was induced when the OD_{600} of the cell culture had reached values between 1.5 or 2. Five milliliter of 1M IPTG solution and 30 mL of 10 mg/mL hemin chloride solution were added to the media after the induction. The cells were grown continuously until two or three constant values of OD_{600} readings were obtained in the stationary phase. Then, the culture was collected and centrifuged for 20 min at 4ºC and 4,000 rpm in a Beckaman J2-HS centrifuge. The bacterial pellet was stored at -50ºC for further lysis and purification procedures.

2.6 Cell Lysate and isolation of the recombinant HbII protein

The rHbII protein was isolated from the cytoplasm of the bacteria before the protein purification. Native Binding Buffer (NBB) with 58 mM dibasic sodium phosphate (Na_2HPO_4), 17 mM monobasic sodium phosphate (NaH_2PO_4) was used as buffer solution for the cell lysis. The bacterial pellet obtained in the centrifugation was weighted and resuspended in approximately 90 mL of NBB per 35 g of bacteria. Two milligrams of lysozyme per gram of bacteria were added to the resuspended pellet. One tablet of protease inhibitor cocktail (4-(2-aminoethyl)benzenesulfonyl fluoride (AEBSF), E-64, bestatin, leupeptin, aprotinin, and EDTA (sodium salt)) per 50 mL of NBB buffer was added to the resuspended pellet to avoid the protein degradation. Then, the mixture was incubated on ice for approximately 1 hr. When a viscous solution was formed, the solution was sonicated for 75 sec at 30% intensity.

The procedure was repeated, with a rest for one minute between each step until the solution returned liquid. The aqueous lysate was centrifuged at 4 ºC, 15,000 rpm for one hr. The sample was stored at ¯56 ºC to be further purified.

2.7 Purification of rHbII

The lysate was purified by metal affinity chromatography using an AKTA FPLC system. Ten milliliters of a cobalt resin were contained in the Talon column. The resin was equilibrated with 10 bed volume (BV) of the equilibrating buffer (50 mM sodium phosphate, 300 mM sodium chloride, pH 7.5) at a flow rate of 4.0 mL/min. Approximately 20mL of lysate were loaded into the column. The resin was washed with NBB buffer (58 mM Na_2HPO4, 0.3 M NaCl, pH 7.5) at a flow rate of 4.0 mL/min making sure that the pressure does not exceed 0.2 MPa. The protein was eluted with buffer (58 mM Na_2HPO4, 0.3 M NaCl, 150 mM imidazole, pH 7.5) and the eluted fractions were collected in the fraction collector. Figure 2.3 shows the chromatogram for the affinity chromatography of rHbII which contains two main bands. The first peak in the chromatogram represents the impurities in the sample. The second peak shows our protein (rHbII) in a mixture with imidazole and salts. A desalting process using an AMICON ultra-filtration cell with an YM-10 membrane was completed to eliminate the salts and imidazole present in the sample. Thus, this process eliminates the shoulder in the band of HbII. The solvent was washed out with deionized water and the rHbII sample was stored at ¯56 ºC for future experiments.

2.8 Purity and concentration of recombinant HbII

A sodium dodecyl sulfate polyacrylamide gel electrophoresis (SDS-PAGE) analysis was performed to verify the purity of the proteins. First, 20 µL of SDS-PAGE standard (Bio-Rad) was added to an eppendorf tube and heated at 32°C for one min. Then, 20 µL of each step of the purification procedure were taken and added to a different eppendorf.

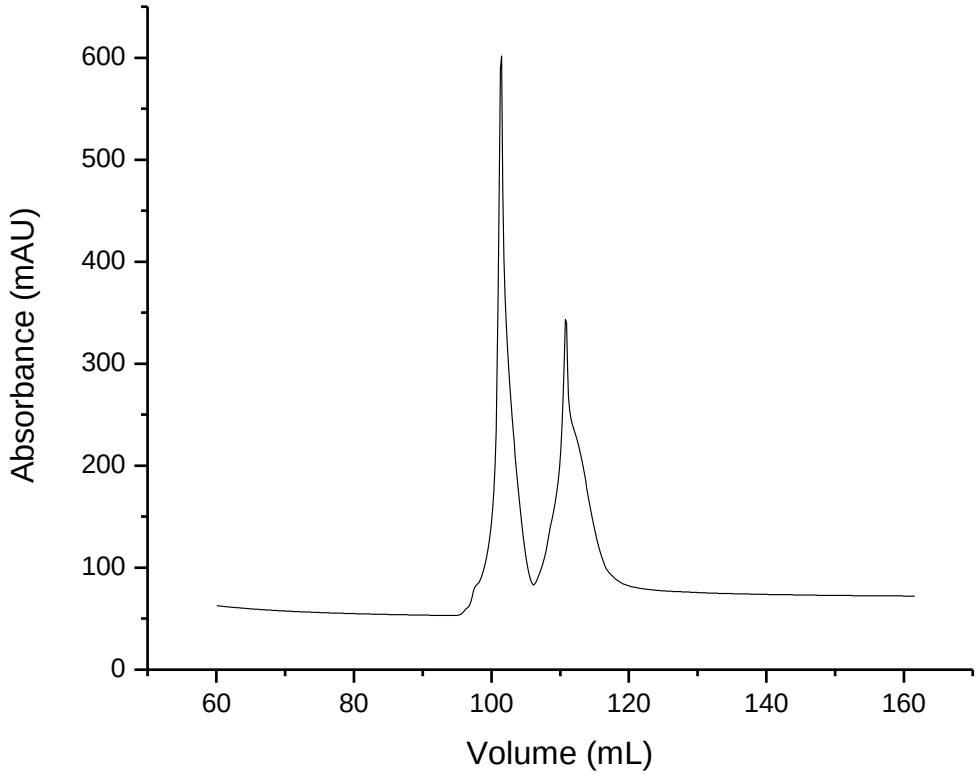

Figure 2.3 Representation of the metal affinity chromatography of recombinant HbII using a FPLC. The first peak in the chromatogram represents the impurities in the sample. The second peak shows a mixture of (rHbII) with imidazole and salts.

Ten microliters of the "running buffer" (1X –Tris, Glycine, SDS) were added to each sample and mixed in a VORTEX. Each sample was heated at 95 °C for 5 min on a sand bath. Then, 16 µL of the samples were injected into the gel. The samples migrated across the gel by applying a constant voltage of 150 V and a current of 114 mA for 45 min using a power supply. After 45 min, it was removed from the system and dyed with Coomasie Blue G-250 for 15 minutes and washed out three times with a 10% acetic acid solution. Then, the gel was placed overnight in deionized water. The next day, the bands were compared with a prestained SDS-PAGE standard (Bio-Rad) with a molecular weight range of 6,900 to 194,239 daltons.

The spectral properties of ferric and ferrous states of HbII were used to determine the hemoglobin concentration (Wittenberg 1990). The concentration of the sample was found using the absorption maxima (λ_{max}) in the UV-Vis region, the corresponding absorptivity coefficients, and the Beer-Lambert Law. The equation 1 was used to determine the sample concentration

$$A = \epsilon\, b\, C \qquad (1)$$

where A is the absorbance at the maximum wavelength (λ_{max}) at the Soret band, b is the pathlength of the cuvette, c is the concentration of the sample and ε is the absorptivity coefficient at the λ_{max}. Table 2.1 summarizes the spectral properties used during the experiments.

Table 2.1: Spectral properties of the HbII complex from *Lucina pectinata*

Derivate	**λ_{max} (nm)**		**ε ($mM^{-1}cm^{-1}$)**	
	Soret band	**Q bands**	**Soret band**	**Q bands**
HbII (deoxy)	432	556	120	12.5
HbII--O_2 (oxy)	414	540	129	13.3
		576		12.6
$HbII^+$ (metaquo)	406	502	130	9.4
		630		3.6

2.9. Formation of the deoxy and carbon monoxide of recombinant HbII

For the preparation of the rHbII complex, approximately 900 μL of rHbII were transferred to a quartz cuvette and tightly sealed with a rubber septum. Also a 200 mM sodium dithionite solution ($Na_2S_2O_4$) was prepared with 100 mM potassium biphosphate buffer solution. Then the rHbII sample and the buffer solution were purged for 15 min with gaseous nitrogen to remove the oxygen present in the sample. The rHbII sample was titrated with the sodium dithionite solution until was observed a displacement in the Soret band from 414 nm to 432 nm. This displacement represents the formation of the deoxy complex. Then of the deoxy complex was formed, the sample was exposed for 5 minutes to a CO atmosphere for the formation of the carbon monoxide complex. The formations of the complexes were verified by UV-Vis spectroscopy. The displacement in the Soret band was observed from 432 nm to 420 nm.

2.10 Formation of the met-hydroxide and met-aquo complex of recombinant HbII

To obtain the met-hydroxide complex of rHbII, the sample was titrated with 30% excess of potassium ferricyanide ($K_3Fe(CN)_6$). First, a UV-Vis spectrum was obtained to confirm that the sample was in the oxy form. The sample was titrated with the $K_3Fe(CN)_6$ solution and variations in the pH were made 0.1 M NaOH to reach a final pH of 11. The formation of the met-hydroxide was observed when the Soret band was displacement from 414 nm to 406 nm. The same procedure was made to obtain the met-acid complex of rHbII, but the variations in the pH were made to a final pH value of 4 with 0.1 M HCl.

2.11 Kinetics of the reactions of rHbII with O_2

The affinity constant, $k_{affinity}$ for the reactions of HbII with oxygen is defined as the ratio of k_{on} / k_{off} in the reversible reaction:

$$HbII(Fe^{II}) + O_2 \underset{k_{off}}{\overset{k_{on}}{\rightleftarrows}} HbII(Fe^{II})\text{-}O_2 \qquad (2)$$

The rate constant for association (k_{on}) and dissociation (k_{off}) of O_2 were determined independently as discussed in the following sections.

2.11.1 Determination of the affinity constant (k_{on})

The oxygen association rate constants, k_{on}, for the recombinant HbII was measured using a rapid scanning monochromator (Olis) with a stopped-flow apparatus. The scans were recorded from one millisecond up to ten seconds. Solutions of 15 μM deoxygenated HbII in Native Binding Buffer (NBB), were mixed rapidly with solutions of O_2 with different concentrations (0.01 mM -- 0.33 mM). The formation of the HbII-O_2 complex was monitored at 414 nm. The observable kinetics constants from the data were calculated using single value decomposition (SVD), global analysis and curve fitting routines included in the Olis software. The following reaction represents the reaction studied for the determination of the association constant:

$$HbII(Fe^{II}) + O_2 \xrightarrow{k_{on}} HbII(Fe^{II})\text{-}O_2 \qquad (3)$$

and it represent a second order reaction with a rate reaction:

$$r = k_{on}\,[HbII][O_2] \qquad (4)$$

Since the experiments were made under flooding conditions $[O_2] >> [HbII]$, the reaction model assumed was from a pseudo first order:

$$r = k_{obs}[HbII] \qquad (5)$$

and

$$k_{obs} = k_{on}\,[O_2] \qquad (6)$$

The pseudo first order constant (k_{obs}) was obtained from the plot of ln (A_t – A □) vs. time. The observable constants were plotted against O_2 concentration to obtain the second order rate constant (k_{on}) for the formation of the HbII-O_2 complex. The k_{on} value is given by the slope of the line obtained from the linear regression analysis.

2.11.2 Determination of the dissociation constant (k_{off})

The dissociation constant, k_{off}, of rHbII was calculated running a time course of the complex HbII-O_2 to see the decay of the signal and the formation of the deoxy complex using a UV-Vis spectrophotometer. An optical cuvette filled with 2 mL of phosphate buffer was deoxygenated under an alternate stream of vaccum and nitrogen. Then, a solution of 6 μM sodium dithionite was prepared in the degassed buffer. One hundred microliters of 5 μM HbII was injected into the cuvette and the oxygen dissociation signal at 414 nm was recorded as a function of time. Kinetic trace was observed using the kinetic mode on the UV-Vis spectrophotometer during one hour. The following reaction represents the reaction studied for the determination of the dissociation constant:

$$HbII(Fe^{II})\text{-}O_2 \xrightarrow[k_{off}]{} HbII(Fe^{II}) + O_2 \qquad (7)$$

and it represent a first order reaction with a rate reaction:

$$r = k_{off}\,[HbII\text{-}O_2] \qquad (8)$$

To determine the k_{off} values, the data was analyzed using the Origin Pro 8.0 software. The mathematical fit which better described the behavior of the experimental data points is the first order exponential decay, represented by

$$y = A_1 \exp^{-x/t1} + y_0 \qquad (9)$$

2.12 Determination of the oxidation constant (k_{ox})

The oxidation constant, k_{ox}, was calculated by running a time course of the complex HbII-O_2 to see the decay of the signal using a UV-Vis spectrophotometer. The HbII-O_2 complex was monitored by observing the Soret and Q bands. An optical cuvette filled with 2 mL of phosphate buffer was deoxygenated under a stream of nitrogen. Then, 5 μL of 0.2 mM HbII was injected

into the cuvette and the oxygen dissociation signal at 414nm was recorded as a function of time. Kinetic trace was observed using the kinetic mode on the UV-Vis spectrophotometer during 24 hours. The following reaction represents the reaction studied for the determination of the autoxidation constant:

$$HbII(Fe^{II})\text{-}O_2 \xrightarrow{k_{ox}} HbII(Fe^{III}) + O_2^{\cdot -} \qquad (10)$$

and it represent a first order reaction with a rate reaction:

$$-r = k_{ox}\,[HbII\text{-}O_2] \qquad (11)$$

RESULTS AND DISCUSSION

3.1 Recombinant HbII transformation

The construction of the rHbII and the insertion of the rHbII cDNA into the pET-28a(+) was performed in the Biochemistry Laboratory of Dr. Carmen L. Cadilla in the U.P.R.-Medical Science Campus in San Juan. The pET-28a(+) plasmid containing the rHbII DNA was transformed in the BLi5 and BL21 cells strain with a high efficiency. After cell transformation, plasmid extractions were performed to analyze the transformed cells. Figure 3.1 shows the 1% agarose gel electrophoresis analysis performed for the DNA of the bacteria to identify which colonies have the rHbII inserts. In the agarose gel, the lane 1 and 10 contain the DNA ladders; lane 1 contains the 123 bp DNA ladder and lane 10 the 1 Kb DNA ladder. The lanes 2-9 show a DNA fragment of approximately 5.4 Kb that corresponds to the linearized pET-28a(+) vector and another fragment of approximately 478bp corresponding to the HbII cDNA. According to Torres et al., 2003, the open reading frame of the HbII full-length cDNA is 459 bp long and the remainders 19 bp in the band correspond to the distance among the *HindIII* site (position 173) and the EcoRI site (position 192) since upon inserting HbII cDNA was utilized *XhoI* and *HindIII* restriction enzymes. Analysis of the cloned samples by restriction enzymes in an agarose gel electrophoresis indicated that the HbII cDNA was successfully cloned. In addition, the DNA sequence obtained demonstrates that the length of the HbII coding region was the same reported previously by Torres et al., 2003. After the transformed cells were identified, a pilot expression test and subsequently large-scale expression experiments were performed. The results of those experiments will be discussed in the following sections.

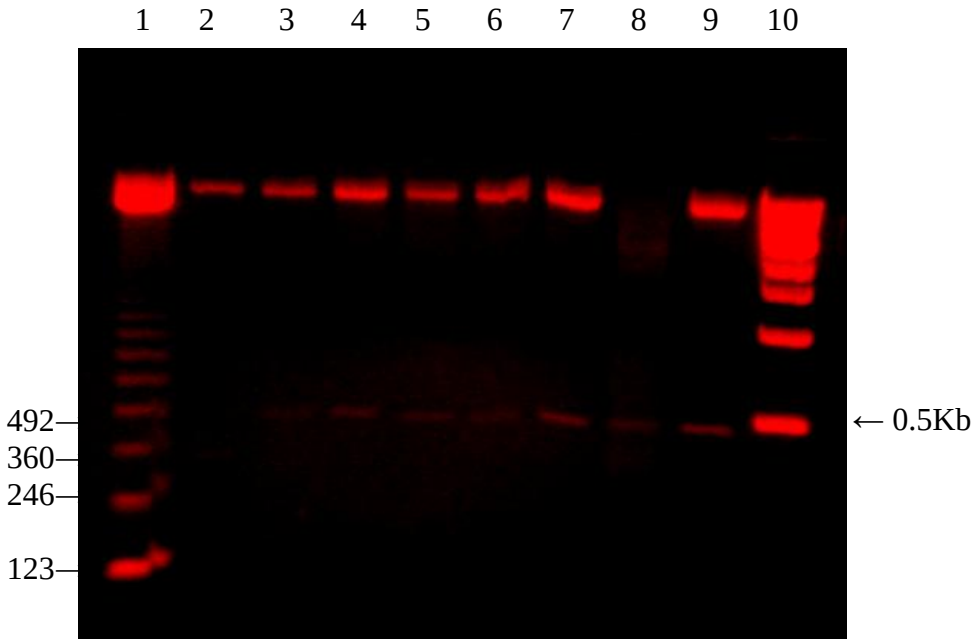

Figure 3.1 Agarose gel electrophoresis of the double enzymatic digestion with EcoRI and XhoI enzymes of the plasmid pET28(a+) containing the rHbII insert. Lane 1 and 10 contain the DNA molecular weight standard; lane 1 contains the 123 bp DNA ladder and lane 10 the 1 Kb DNA ladder. Lanes 2-9 show the expected bands of rHbII DNA after the double enzymatic digestion.

3.2 Recombinant HbII expression

To determine the optimal conditions for rHbII expression in our study, the rHbII levels were examined in 1L Fernbach cultures. In these experiments a series of different conditions were examined such as: time induction, temperature after induction, and the bacterial strain. After evaluating these conditions and with the purpose of producing the protein in a large scale expression, a 5 L Benchtop Fermentator was used.

3.2.1 Effect of the time induction during the rHbII expression

The first parameters studied to determine the optimal conditions for the protein expression was the time induction. Pilot expressions of 1 L were performed using the BL21 and BLi5 *E. coli* cells and the pET28(a+) plasmid containing the cDNA of rHbII. Previous studies made by Leon et al., 2004 demonstrated that the high protein yield occurs when the expression was induced during the end of the log phase ($OD_{600} \sim \geq 1.4$), but studies made by Jung et al., 2001 reported a new system to obtain high protein expression when the induction was performed during the log phase. In our studies, for the expression experiments induced when the OD_{600} was less than 1.4 (log phase), the amount of protein obtained was 33.60 mg/L for the BL21 cells and 41.73 mg/L for the BLi5 cells. For the expression experiments induced after the log phase (OD_{600} 1.4-2.0), the amount of protein was 116.57 mg/L for the BL21 cells and 154.67 mg/L for the BLi5 cells. Figure 3.2 shows the SDS-PAGE electropherogram for the detection of rHbII at different induction time. In the polyacrylamide gel, lane 1 contains the SDS-PAGE standard and the lanes 2-5 show the detection of rHbII, which has a theoretical molecular weight of 16,128 daltons, at different induction time. The lanes 2-3 show the rHbII detection when the induction time was less than 1.4 and lanes 4-5 when the induction was after the log phase (OD_{600} 1.4-2.0).

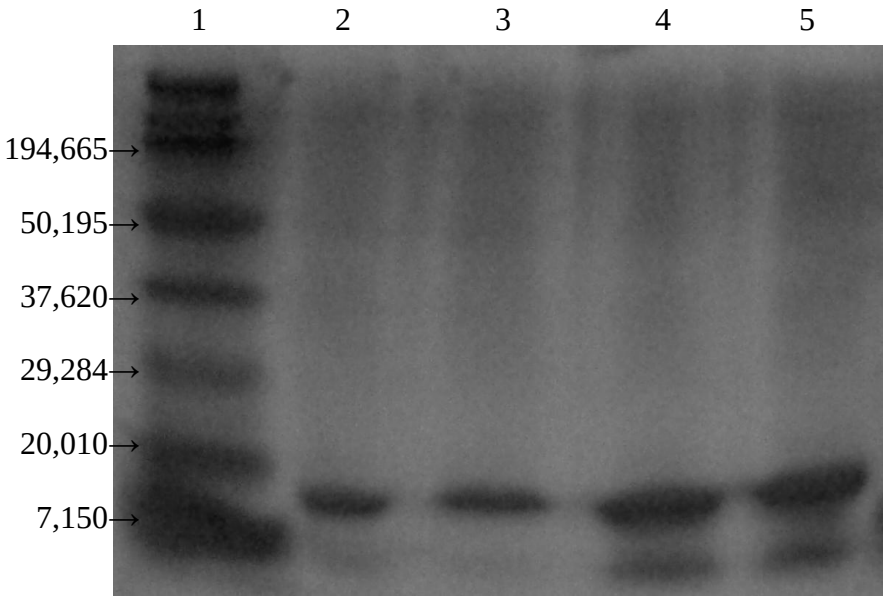

Figure 3.2: Sodium dodecyl sulfate polyacrylamide gel electrophoresis (SDS-PAGE) analysis for the detection of rHbII at different induction time. Lane 1 contains the SDS-PAGE standard and the lane 2-5 show the detection of rHbII, which has a theoretical molecular weight of 16,128 daltons, at different induction time. The lanes 2-3 show the rHbII detection when the induction time was less than 1.4 and lanes 4-5 when the induction was after the log phase (OD_{600} 1.4-2.0)

When we compared the amount of purified protein obtained at the different time of induction, the better yield was obtained when the protein expression was induced after the log phase (OD_{600} 1.4-2.0) and the BLi5 cells was used for the protein expression. Although, previous studies show that the better protein yield was obtained in the log phase. In our studies we obtained the high protein yield during the induction to OD_{600} 1.4-2.0. A probable reason for this result would be that during the log phase the cells were in the replication mode and the bacterial were competing. Otherwise, after the log phase, the media had more bacteria ready to express rHbI and the expression was the principal process occurring in the media (Leon et al., 2004).

Table 3.1 Protein yield of rHbII in *E. coli* BL21 and BLi5 cells at different induction times.

Induction time	**Amount of purified protein**	
OD_{600}	**BL21 cells**	**BLi5 cells**
Less than 1.4	33.60 mg/L	41.73 mg/L
1.4 — 2.0	116.57 mg/L	154.67 mg/L

3.2.2 Effect of the temperature in the protein yield

To determine the optimal induction time, the next variable that we studied to improve the protein yield was the temperature of induction. These experiments were performed using the BL21 and BLi5 *E. coli* cells and the pET28(a+) plasmid containing the cDNA of rHbII. Pilot expressions of 1 L and induced at an OD_{600} of 1.4-2.0 were carried out to determine the protein concentration at temperatures of 25 °C, 30 °C, and 37 °C after induction. Previous studies demonstrated that a lower temperatures, the percent of soluble protein yield is better than with higher temperatures (Weickert et al., 1997; Leon et al., 2004). For the experiments performed at 25 °C, the amount of protein obtained was 17.89 mg/L for the BL21 cells and 18.72 mg/mL for the BLi5 cells. At 30 °C, for the BL21 cells, the amount of obtained protein was 130.30 mg/L and 134.72 mg/L for the BLi5 cells. And for the experiments carried out at 37 °C, the amount of protein was 101.78 mg/L for the BL21 cells and 104 mg/L for the BLi5 cells. Figure 3.3 shows the SDS-PAGE electropherogram for the detection of rHbII at different temperatures of induction. In the polyacrylamide gel the lanes 1 and 8 contain the SDS-PAGE standard and the lanes 2-7 show the detection of rHbII at different temperatures of induction. The lanes 2-3 show the rHbII detection when the induction temperature was 25 °C; lanes 4-5 when the induction temperature was 30 °C and lanes 6-7 when the induction temperature was 37 °C. When we compared the amount of purified protein obtained at the different temperatures, the better yield was obtained when the temperature after the induction was 30 °C and the BLi5 cells was used for the protein expression.

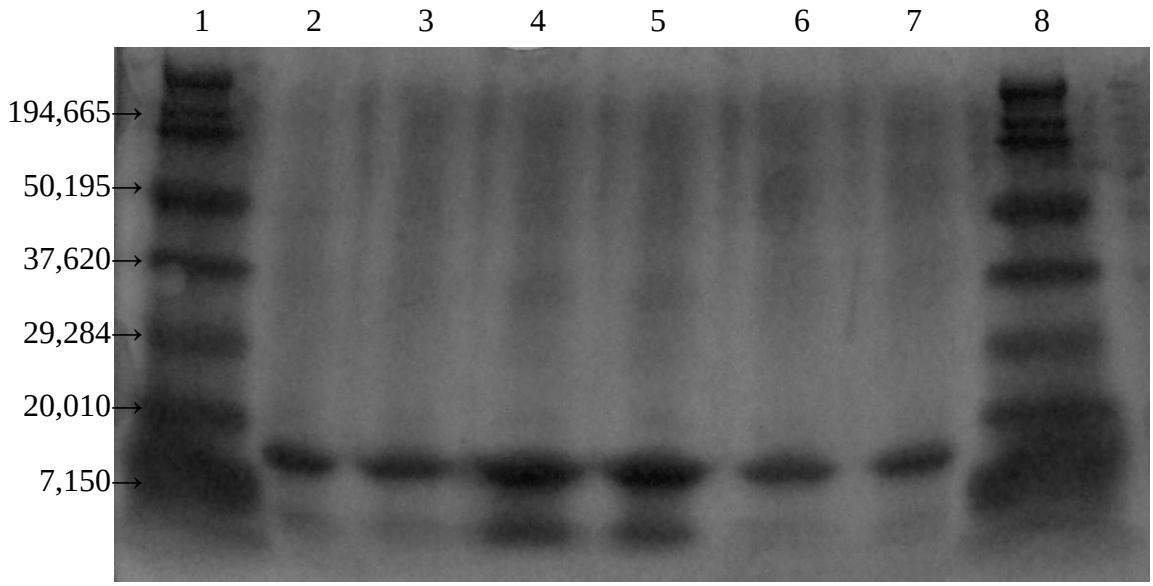

Figure 3.3: Sodium dodecyl sulfate polyacrylamide gel electrophoresis (SDS-PAGE) analysis for the detection of rHbII at different temperature of induction. Lanes 1 and 8 contain the SDS-PAGE standard and the lanes 2-7 show the detection of rHbII at different temperature of induction. The lanes 2-3 show the rHbII detection when the induction temperature was 25 °C; lanes 4-5 when the induction temperature was 30 °C and lanes 6-7 when the induction temperature was 37 °C.

Table 3.2 Protein yield of rHbII in *E. coli* BL21 and BLi5 cells at different temperature of induction.

Temperature (°C)	Amount of purified protein	
	BL21 cells	BLi5 cells
25	17.89 mg/L	18.72 mg/L
30	130.30 mg/L	134.72 mg/L
37	101.78 mg/L	104 mg/L

3.2.3 Effect of the bacterial strains: BL21 and BLi5 *E. coli* strains

Experiments used two different bacterial strains, the BL21 and BLi5 *E. coli*, were performed to improve the protein expression. Pilot expressions of 1 L of both strains induced at an OD_{600} of 1.4 ~ 2.0 were carried out to determine the protein concentration at a temperature of induction of 30°C. For the experiments performed with the BL21 cells the amount of protein obtained was 104.21 mg/L and for the BLi5 cells 125.36 mg/L. These results show that when the expression was performed with the BLi5 *E. coli* strain, the protein yield was better (Figure 3.4). The differences between these two strains are that the *E. coli* BLi5 cell strain was prepared by inserting the pDIA17 plasmid containing the lacI repressor into the BL21 cell strain. This repressor maintains the recombinant protein expression strongly repressed until it is induced with IPTG and for this reason a better protein expression was obtained when this *E. coli* cell strain was used (Munier et al., 1991).

Table 3.3 Protein yield of rHbII in *E. coli* BL21 and BLi5 cells.

E. coli strain	Amount of purified protein
BL21	104.21 mg/L
BLi5	125.36 mg/L

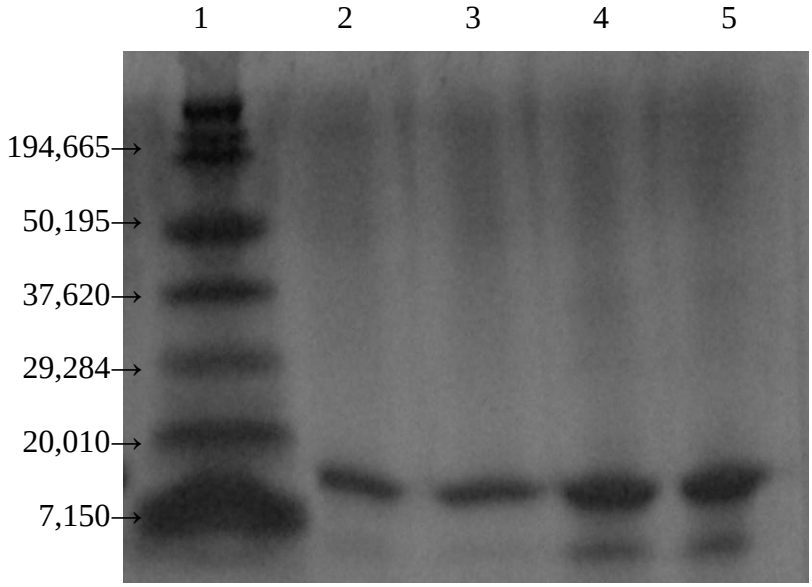

Figure 3.4: Sodium dodecyl sulfate polyacrylamide gel electrophoresis (SDS-PAGE) analysis for the detection of rHbII when different *E. coli* strains were used. Lane 1 contains the SDS-PAGE standard and the lanes 2-5 show the rHbII samples. The lanes 2-3 show the rHbII detection when the BL21 *E. coli* strain was used and lanes 4-5 when the BLi5 *E. coli* strain was used.

3.2.4 Overexpression of rHbII

The high level expression of rHbII was possibly by the transformation of the pET28(a+) plasmid into the BLi5 *E. coli* competent cells. The protein expression was performed in a 5L fermentator and achieved after 10 hours of expression reaching an OD_{600} of 60. Figure 3.5 shows the sigmoid bacterial growth curve of the rHbII that was constructed with the optical density taken each 30 min. The medium used for the expression process was the TB which provided the nutrient necessary for the bacterial growth. During the expression process, the conditions for the optimum bacterial growth were controlled and the vessel was maintained at pH 7 and 35% of dissolved oxygen. The culture was induced when it reached to an OD_{600} of 1.4-2.0. The temperature of the vessel was maintained at 37°C before the induction and after the induction it was reduced to 30°C to improve the protein expression. Additions of 1 mM IPTG and 10 mg/mL hemin chloride solution were performed at the beginning of the logarithmic phase and the protein expression continued until the stationary phase reached. Previous studies demonstrated that the addition of hemin chloride to the cell pellet lysate improves the heme incorporation, but aggregation problems are encounter (Rosado-Ruiz et al., 2001; Collazo-Velez et al., 2004). Nevertheless studies made by Leon et al., 2004 and coworkers show that the addition of hemin chloride at the time of induction improves the heme incorporation during the protein expression and aggregation problems are not encounter (Leon et al., 2004).

3.3 Purification of the expressed protein

The bacterial lysis was performed in the presence of a protease inhibitor cocktail, lysozyme and NBB buffer. The crude extract was loaded in a metal affinity chromatography with a cobalt resin and an imidazole gradient was used to elute the protein (Leon et al., 2004).

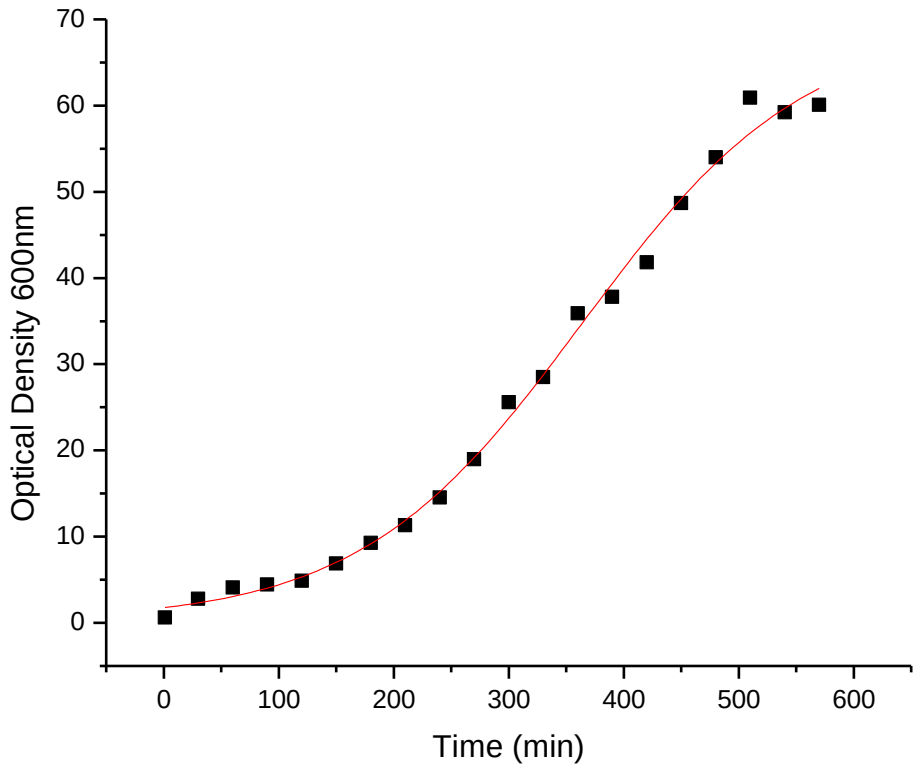

Figure 3.5 Sigmoid bacterial growth curve of the rHbII expressed in BLi5 *E. coli* cells. The bacterial growth is represented by a curve that consists of three phases: lag phase, log phase and stationary phase and each points of the curve is a measure of the optical density in a 30 min interval.

Figure 3.6 shows each step in the purification of recombinant HbII from *Lucina pectinata* after bacterial lysis, demonstrating the protein expression. In the SDS-PAGE electropherogram, Lanes 1 and 8 contain the SDS-PAGE broad range molecular weight standard and the lanes 2-7 show each steps of purification. Lane 2 contains the crude lysate; lane 3 contains sample of the pass through steps; lane 4 contains sample of the wash step; lane 5 contains sample of the elution steps before appear the HbII band and lanes 6 and 7 contain rHbII after purification. At the end of the purification, a UV-Vis spectrum was obtained to monitor the Soret and Q bands to verify the heme insertion. Figure 3.7 shows the spectrum obtained for rHbII after the bacterial lysis and purification. The spectrum shows a Soret Band at 414nm and Q bands at 540nm and 576nm, as expected when the protein is in the oxy form (Wittenberg 1990). The concentration of rHbII was determined by UV/Vis spectroscopy, using the absorption coefficient; 129 mM at 414 nm.

3.4 Reaction of rHbII with ligands (O_2, CO)

To verify the heme group insertion and the spectroscopic characteristic of recombinant HbII, different ligand complexes were formed as show in Figure 3.10 and 3.11. The Figure 3.7, demonstrate that after the protein purification, the collected spectra shows a Soret band at 414 nm and a Q bands at 540 nm and 576 nm corresponding to the low spin oxy-Fe^{II}HbII form of wild type HbII (Wittenberg et al., 1990). The oxy rHbII solution was treated with traces of sodium dithionite showing a displacement of the Soret band to 432 nm, the absence of the Q bands and the formation of a new Q band in 556 nm. As is observed in the spectrum of Figure 3.8, this displacement in the Soret band indicates that when the oxy-Fe^{II}HbII was treated with sodium dithionite, no ligand is binding to the heme group corresponding to a deoxy-Fe^{II} species.

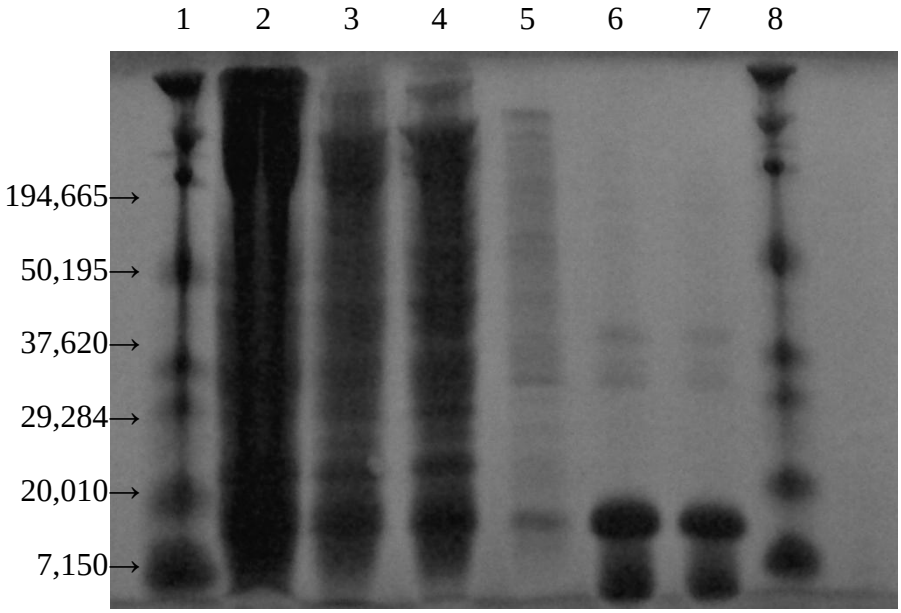

Figure 3.6: Sodium dodecyl sulfate polyacrylamide gel electrophoresis (SDS-PAGE) analysis of each steps of the recombinant HbII purification. The purification process was performed using metal affinity chromatography with a cobalt resin. Lanes 1 and 8 contain the SDS-PAGE broad range molecular weight standard age and the lanes 2-7 show each steps of purification. Lane 2 contains the crude lysate; lane 3 contains sample of the pass through steps; lane 4 contains sample of the wash step; lane 5 contains sample of the elution steps before appear the HbII band and lanes 6 and 7 contains rHbII after purification.

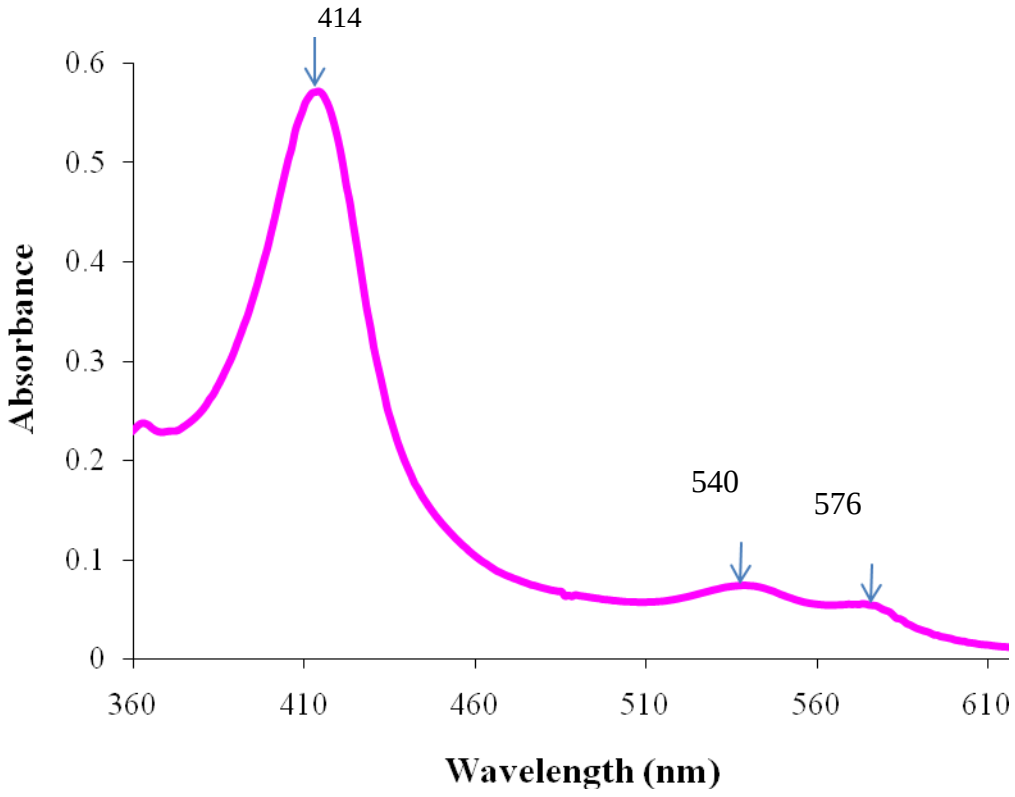

Figure 3.7 UV-Vis spectra of the oxy rHbII obtained after TALON purification. The spectrum shows a Soret band at 414nm and Q bands at 540 and 576 nm identical to wild type HbII-O_2 indicating that the heme group was incorporated during the expression process.

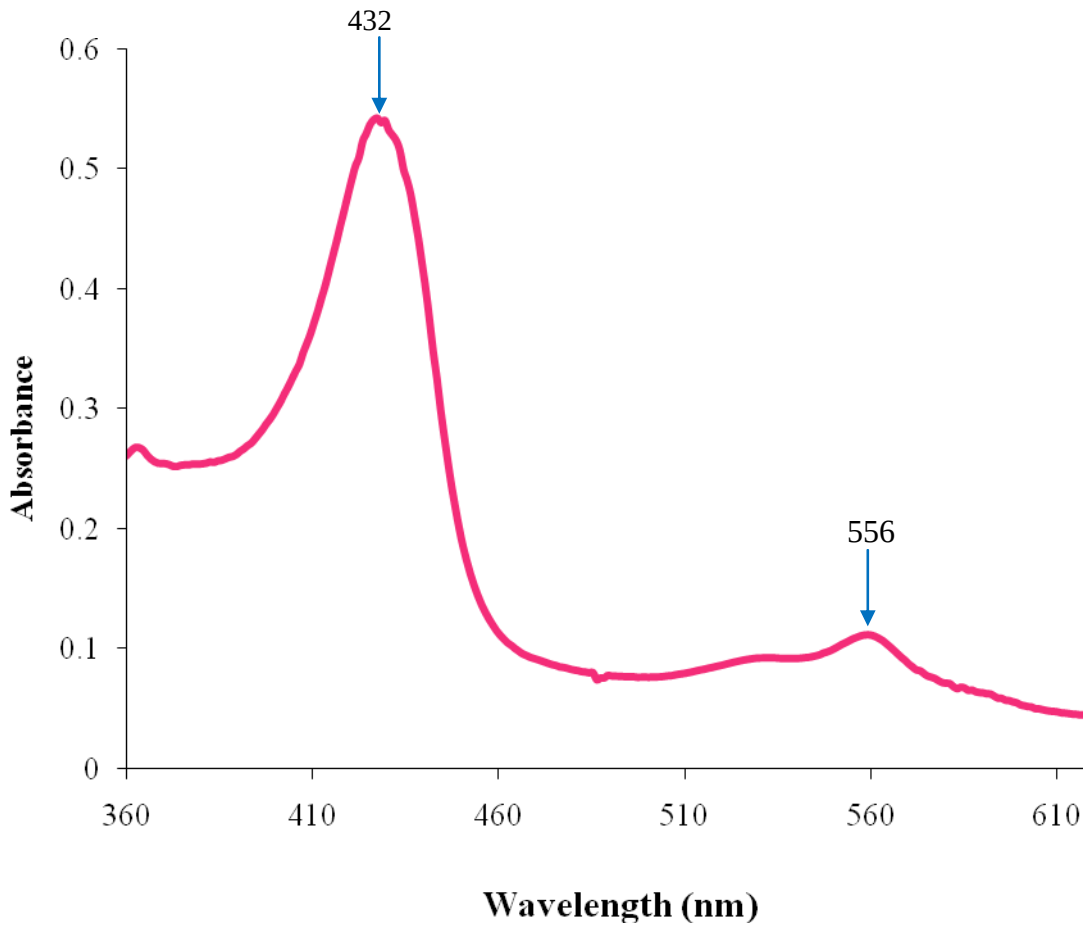

Figure 3.8 UV-Vis spectra of the formation of the deoxy rHbII complex obtained after TALON purification. The spectrum shows a Soret band at 432nm and Q bands at 556 nm identical to wild type HbII. To obtained this spectra the rHbII sample was treated with sodium dithionite.

Then it was exposed to a carbon monoxide atmosphere for five min. Figure 3.9 shows the spectra obtained after the exposition of the sample to the CO atmosphere. As illustrate, the Soret band and the Q bands were displaced to 420 nm and 539 nm and 570 nm, respectively. The Soret bands maxima and Q bands values occurred at wavelength close observed to the wild type HbIIFe^{II}CO complex (Wittenberg et al., 1990). According to the information presented in the several UV-Vis spectra it can be conclude that different ligand complexes were formed, demonstrating that rHbII was able to bind the same ligands as the wild type HbII.

Table 3.4: Summary of the spectral properties obtained for the formation of the rHbII complex with the different ligands.

	Inicial sample (oxy-Fe^{II}HbII)	**Treated with sodium dithionite (deoxy-Fe^{II})**	**Exposed to a carbon monoxide atmosphere (HbIIFe^{II}CO)**
Soret band	414nm	432nm	420nm
Q bands	540 and 576 nm	556nm	539 and 570nm

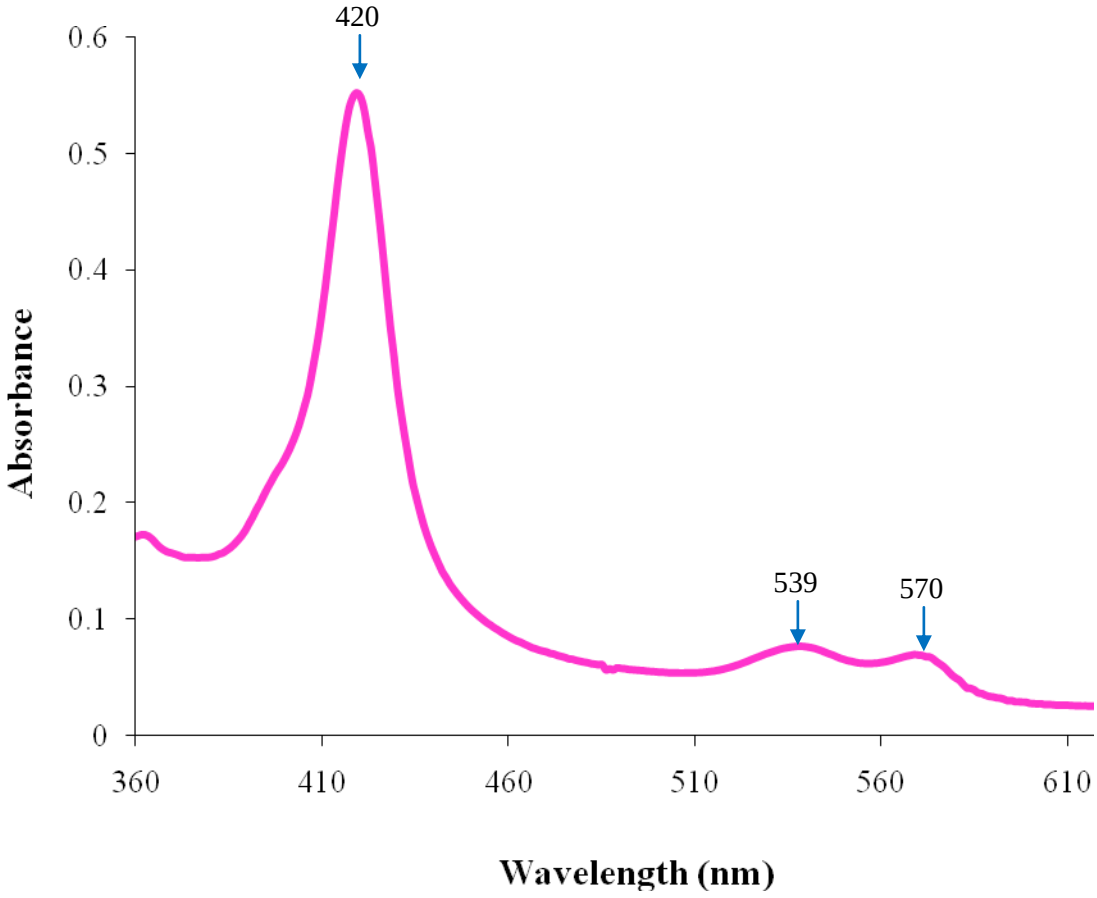

Figure 3.9 UV-Vis spectra of the formation of the rHbII-CO complex obtained after TALON Purification. The spectrum shows a Soret band at 420nm and Q bands at 539 and 570 nm identical to wild type HbII-CO. To obtained this spectra the rHbII sample was treated with sodium dithionite and exposed to a CO atmosphere.

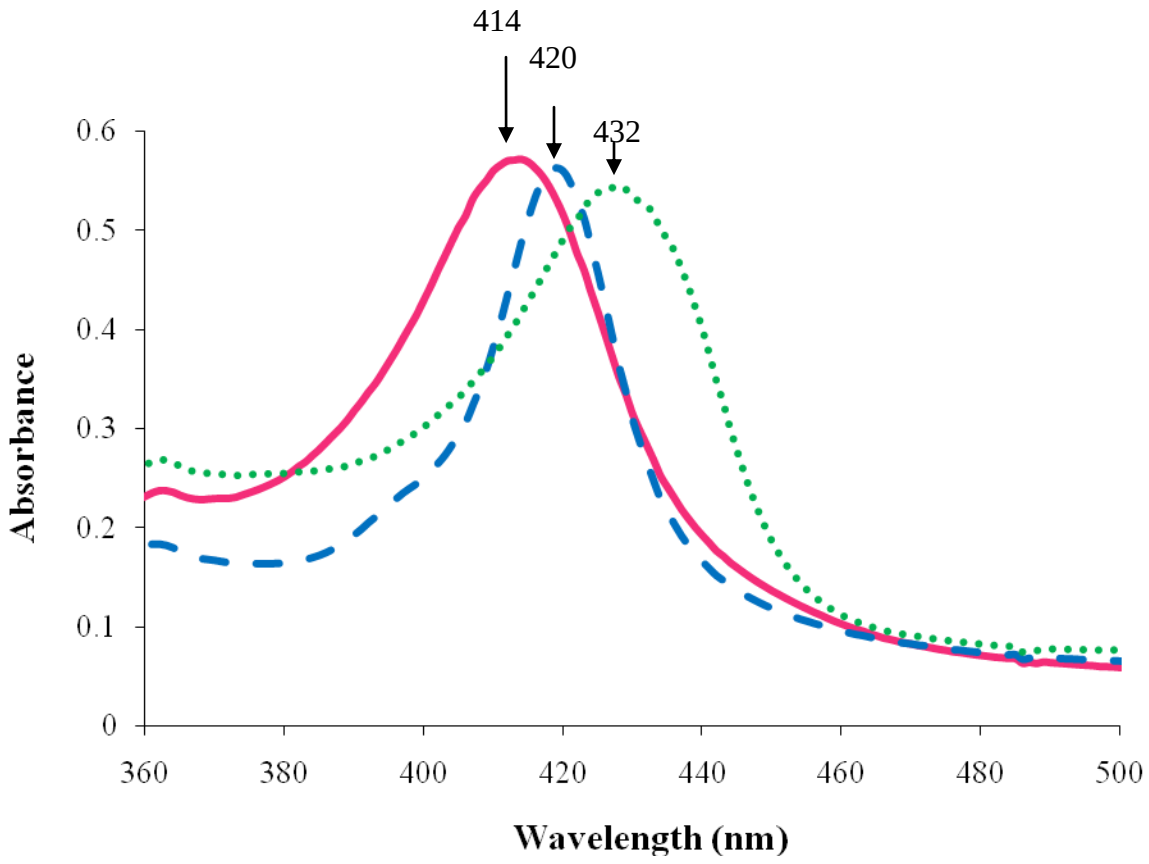

Figure 3.10 UV-Vis spectra of the Soret bands for the carbon monoxide (- -), deoxy (. .) and oxy (——) rHbII complex.

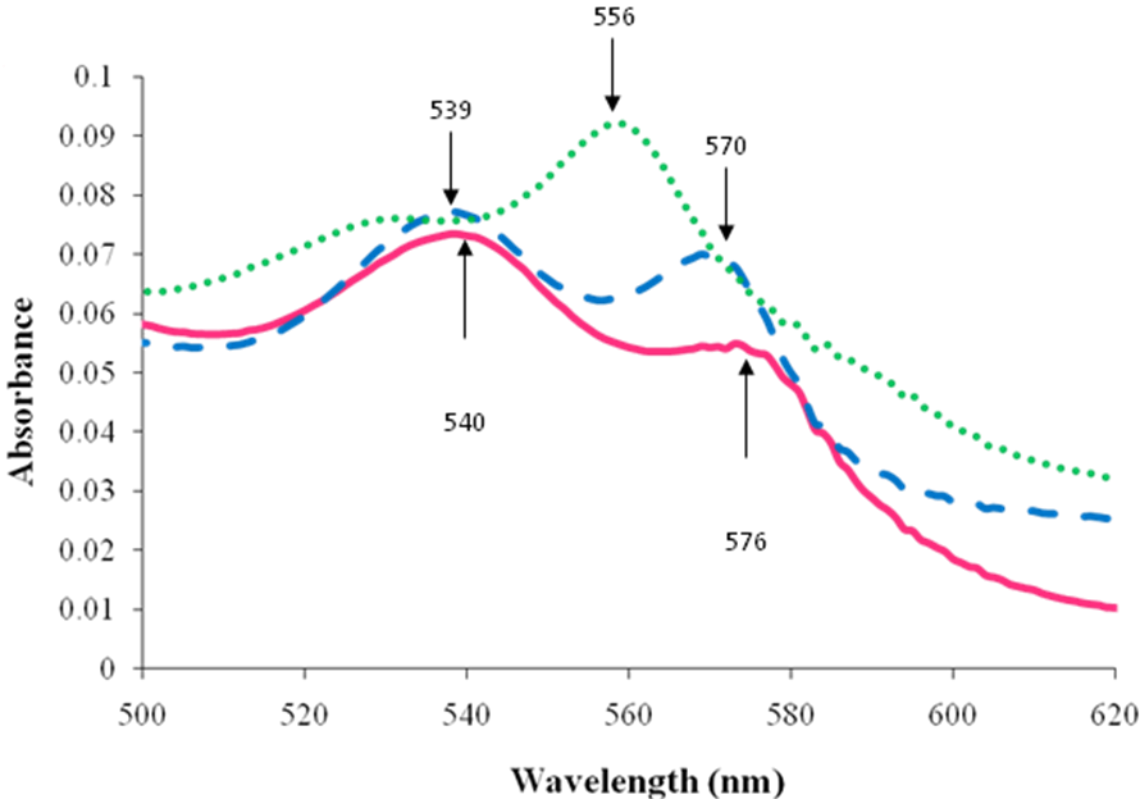

Figure 3.11 UV-Vis spectra of the Soret bands for the carbon monoxide (– –), deoxy (. .) and oxy (——) rHbII complex.

3.5 Formation of the met-hydroxide and met-aquo complex of rHbII

For the formation of the met-aquo specie, the solution was initially titrated with 30% excess of potassium ferricyanide ($K_3Fe(CN)_6$). Then variations in pH from 6.5 to 4 in intervals of 0.5 were made to observe the formation of the met-aquo species and the decay of the oxy species. Spectra measurements were made after 2 min of the 0.1 M HCl addition. Figure 3.12 present the absorption spectra obtained during the titration of a met HbII sample with HCl 0.1 M. The formation of the ferric rHbII at acid pH was evidenced by the disappearance of the band associate with the oxy specie (414 nm, 540 nm, and 576 nm) and the formation of the met-aquo specie (406 nm, 502 nm, and 630 nm) (Pietri et al., 2005).

For the formation of the met-hydroxide specie variations in pH from 4.0 to 11 in interval of 0.5 were made to observe the formation of the met-hydroxide specie and the decay of the oxy specie. Figure 3.13 and 3.14 show the absorption spectra obtained during the titration of the met HbII sample with NaOH 0.1 M. All the spectra measurements were made after 2 min of the 0.1 M NaOH addition. The formation of the ferric rHbII at alkaline pH was evidenced by the formation of the met-hydroxide species (420 nm, 541 nm, and 577nm) and the disappearance of the band associate with the met-aquo species (406 nm, 502 nm, and 630 nm) (Pietri et al., 2005). As was observed in Figure 3.14, rHbII shows the 605 band at neutral to alkaline pH range (~6-9.5) as wtHbII. The formation of this band demonstrated that rHbII form the two species that coexist in constant proportion; the six-coordinated derric hydroxide HbII and the ferric tyrosinate-ligated HbII (Pietri et al., 2005). According to the information presented in the several UV-Vis spectra it can be concluded that the tyrosine B10 and heme-ligand interactions in the rHbII is similar to the interaction in wild type HbII (Pietri et al., 2005).

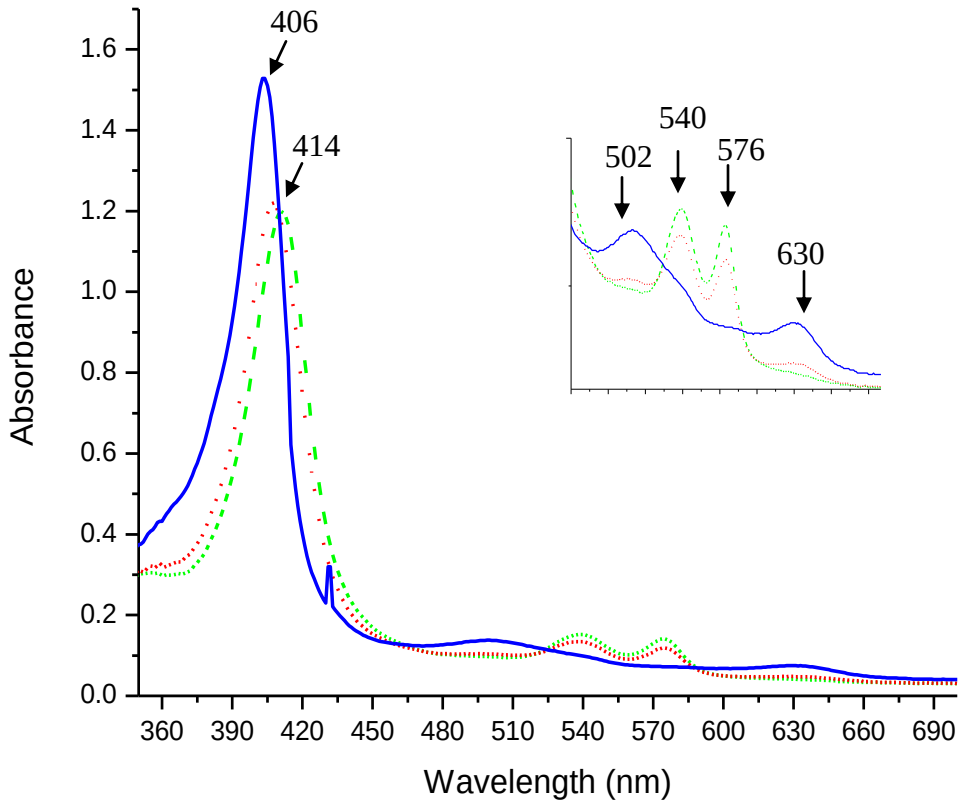

Figure 3.12 UV-Vis spectra of the formation of the met-acid rHbII complex. The complex formation was monitored at different pH: 6.5 (- -), 5.0 (. . .), and 4.0 (——). Spectra measurements were made after 2 min of the 0.1 M HCl addition.

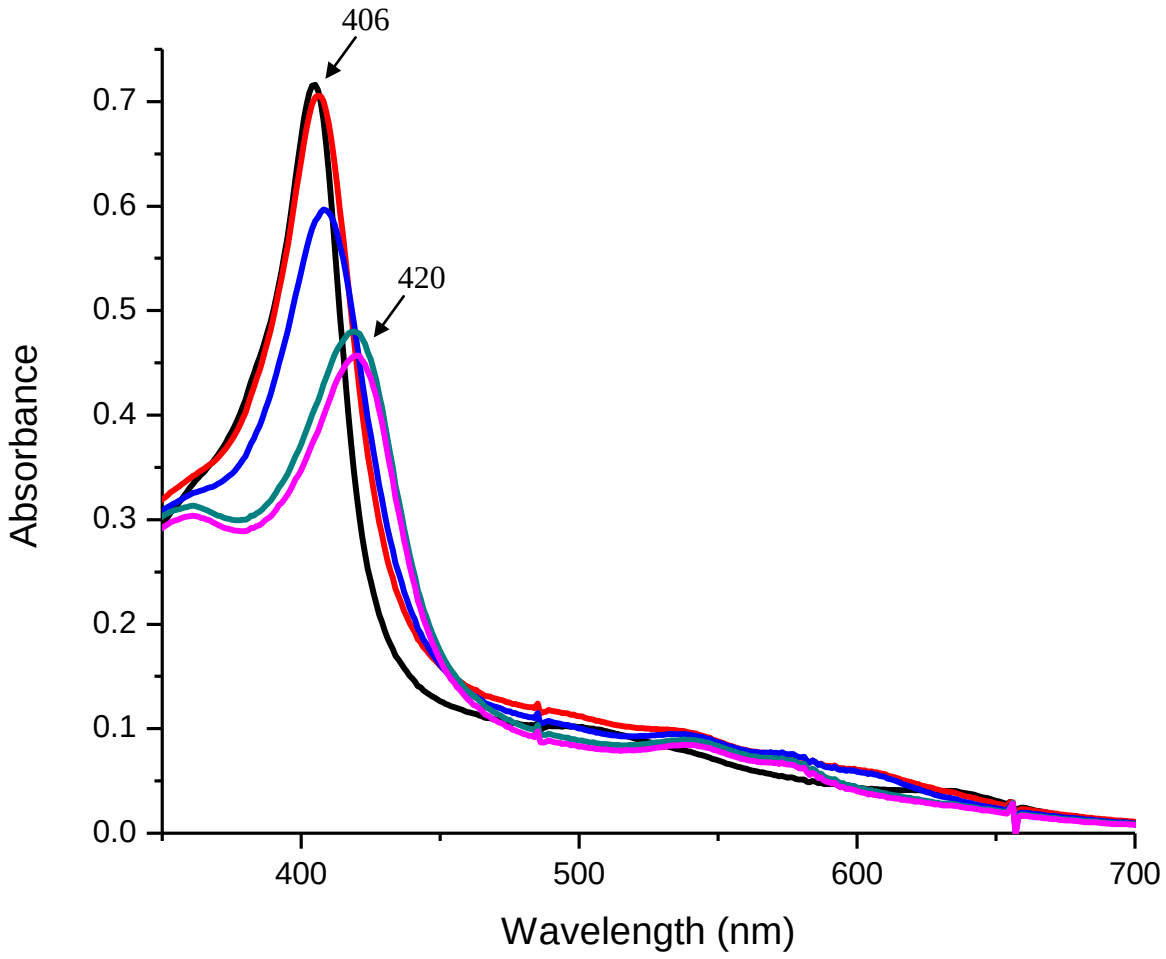

Figure 3.13 UV-Vis spectra of the formation of the met-hydroxide rHbII complex. The complex formation was monitored at different pH: 4.0 (----), 7.5 (- -), 8.5 (---), 10.5 (---) and 11.0 (—). Spectra measurements were made after 2 min of the 0.1 M NaOH addition.

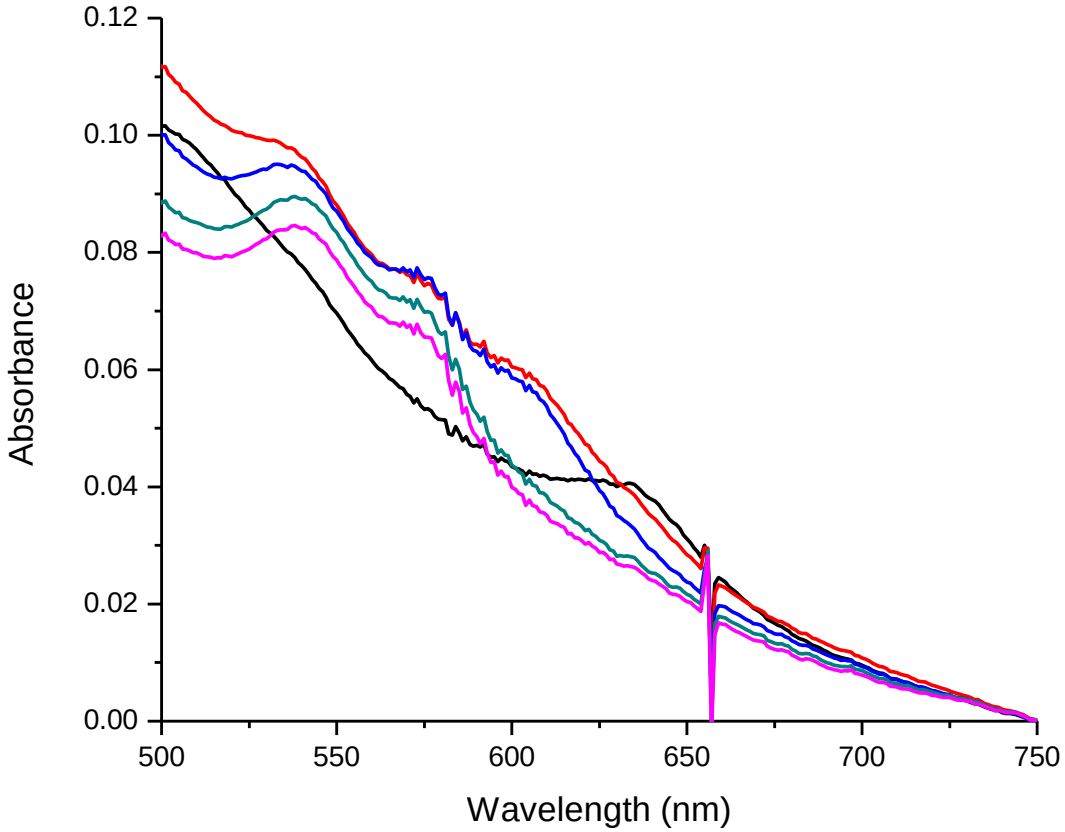

Figure 3.14 UV-Vis spectra of the Q bands for the formation of the met-hydroxide rHbII complex. The complex formation was monitored at different pH: 4.0 (--), 7.5 (- -), 8.5 (--), 10.5 (---) and 11.0 (—). Spectra measurements were made after 2 min of the 0.1 M NaOH addition.

3.6 Kinetics analysis of rHbII with O_2

3.6.1 Oxygen association

To determine the association rate constant for O_2 in rHbII, the kinetic trace was measured using a stopped-flow rapid scanning monochromator spectrophotometer apparatus. The formation of the HbII-O_2 complex was monitored by the appearance of the Soret band at 414 nm and the disappearance of the Soret band at 432 nm (deoxy derivative). The formation of the oxy complex follows a second order reaction and the rate is expressed as k_{on}[HbII][O_2]. But when, we work under flooding conditions [O_2] >> [HbII], the reaction model assumed is a pseudo first order and the pseudo first order constant is expressed as $k_{obs}=k_{on}[O_2]$. Figure 3.15 shows the kinetic trace for the formation of the rHbII-O_2 complex observed at different O_2 concentrations (10 μM —345 μM) for 0.25 seconds. The obtained data were analyzed using the Origin Pro 8.0 software, to determine the k_{obs} value for each oxygen concentrations. To obtain the k_{obs} value was necessary to graph the negative absorbance against the time (Figure 3.16). The mathematical fit used to find the rate constant was the first order exponential decay analysis represented by the equation $y = A_1 \exp^{(-t_1/x)} + y_0$, where 1/x is the first order decay constant (k_{obs}), and the y_0 represent the A_∞. Figure 3.17 shows the kinetic traces for the reaction of rHbII and a concentration of 325 μM of oxygen, the black points represent the experimental data, the red line the first order exponential decay fit and the red points represent the residual plot analysis for the data set, which tells us the proximity between the experimental data and the model used. Similarly, figures 3.17 to 3.21 show the analogues kinetic traces for the reaction between rHbII and O_2, when [O_2] was 141 mM, 61 mM, 23 mM, and 10 mM. For each kinetic trace, a k_{obs} value was obtained by the first order exponential decay equation. Table 3.6 shows the k_{obs} values for wild type hemoglobin II and recombinant HbII at different O_2 concentrations.

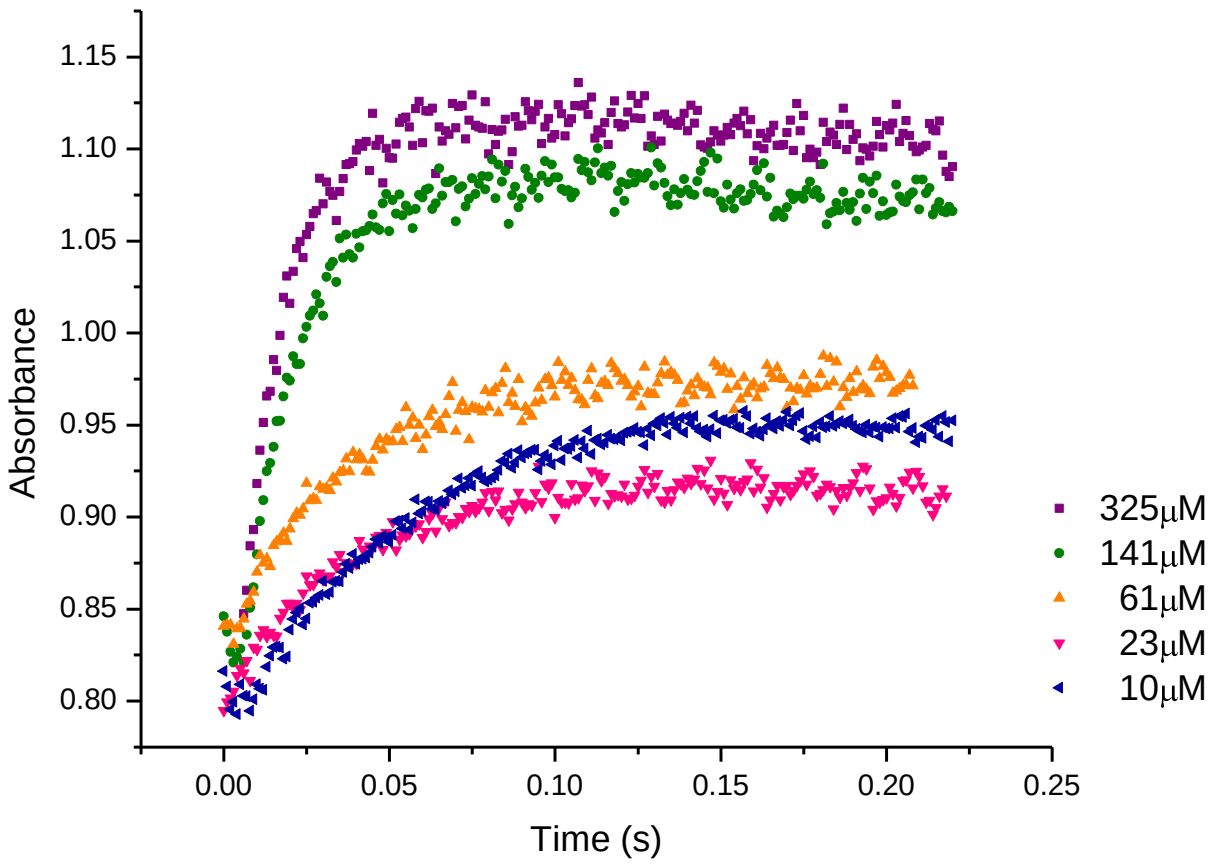

Figure 3.15 Kinetic trace for the O_2 association of the recombinant HbII. The kinetic was followed at 414 nm in a stopped-flow apparatus. All these data were collected for 0.25 sec at a rate of 1000 scans/sec.

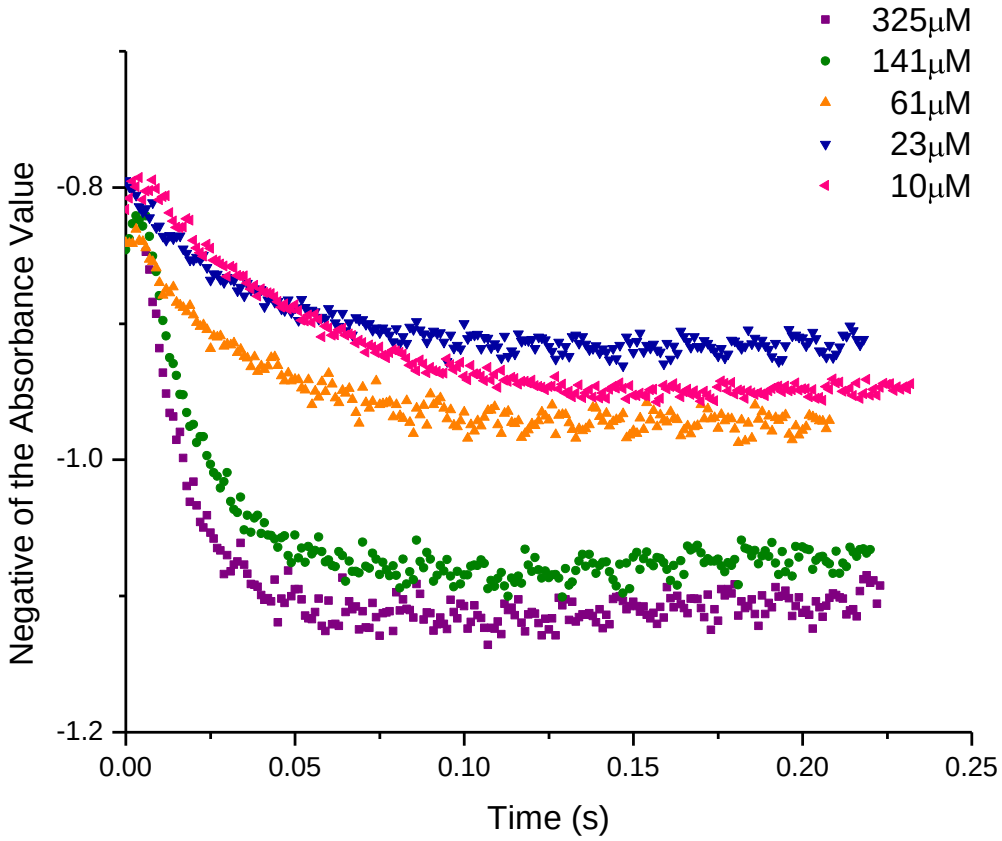

Figure 3.16 Plot of the negative of the absorbance values against time for rHbII. The negative of the absorbance values are used to make the exponential fit of the kinetic model.

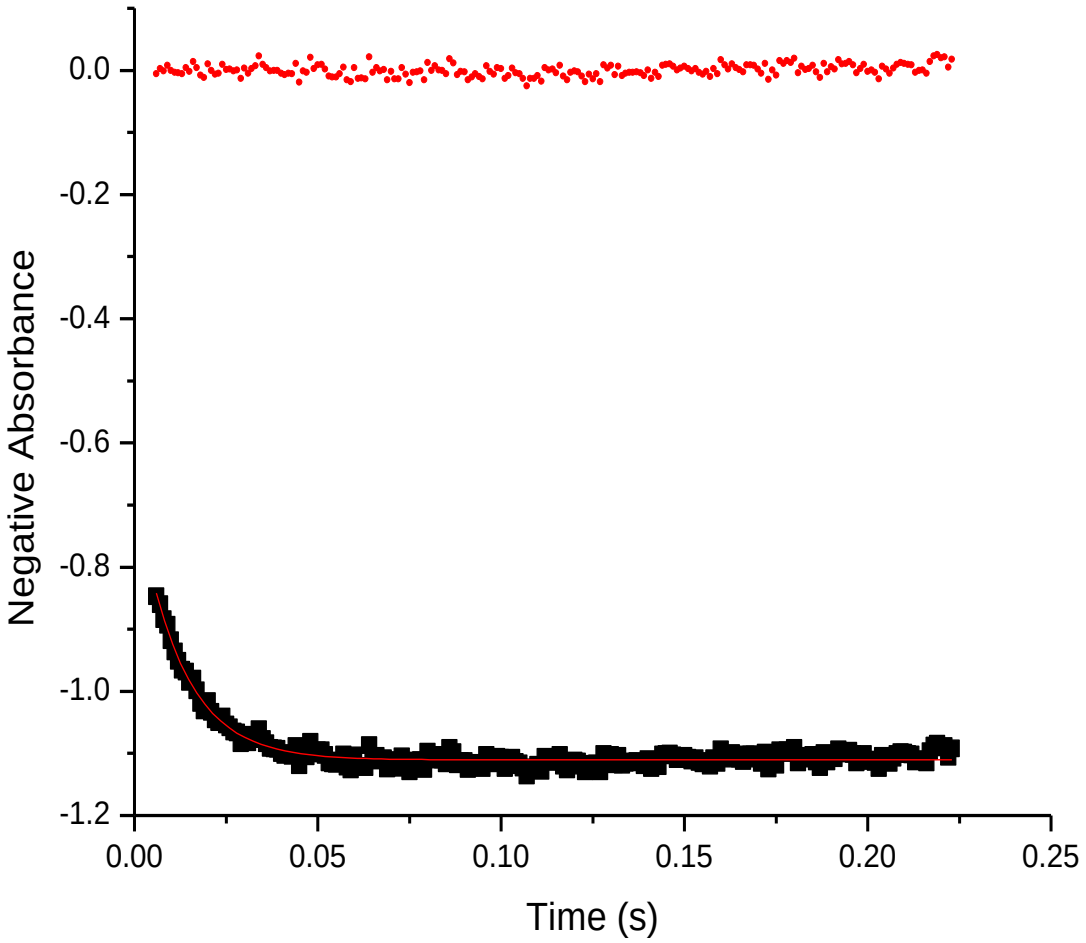

Figure 3.17 Plot of the negative of the absorbance values against time for rHbII at a concentration of 325 μM of an oxygen solution. The red dots represent a residual plot for the experimental data set. The red line represents the exponential decay analysis which is described by the following equation, $y = 0.4421\, e^{(-83.06t)} - 1.111$

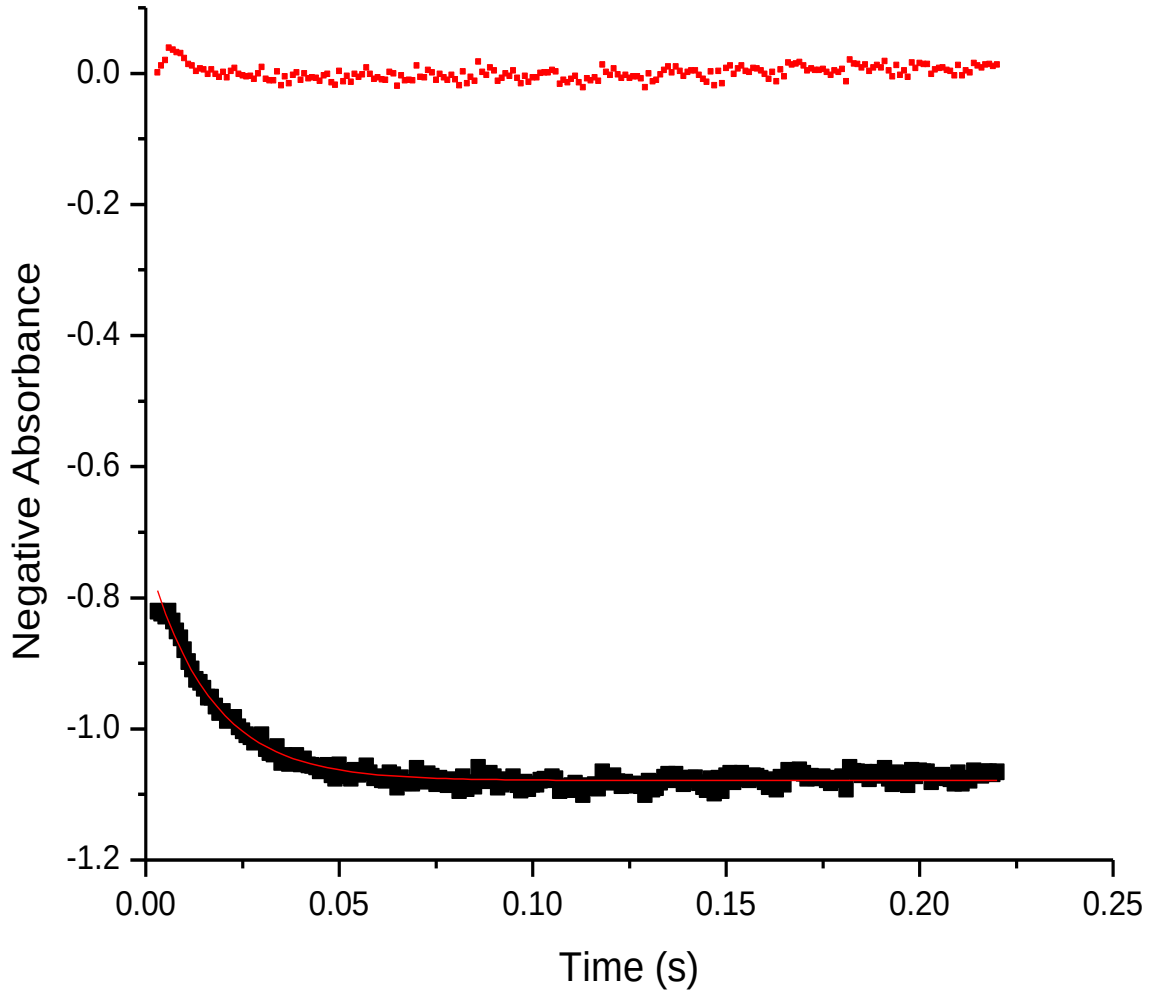

Figure 3.18 Plot of the negative of the absorbance values against time for rHbII at a concentration of 141 μM of an oxygen solution. The red dots represent a residual plot for the experimental data set. The red line represents the exponential decay analysis which is described by the following equation, $y = 0.3025\ e^{(-53.50t)} - 1.080$

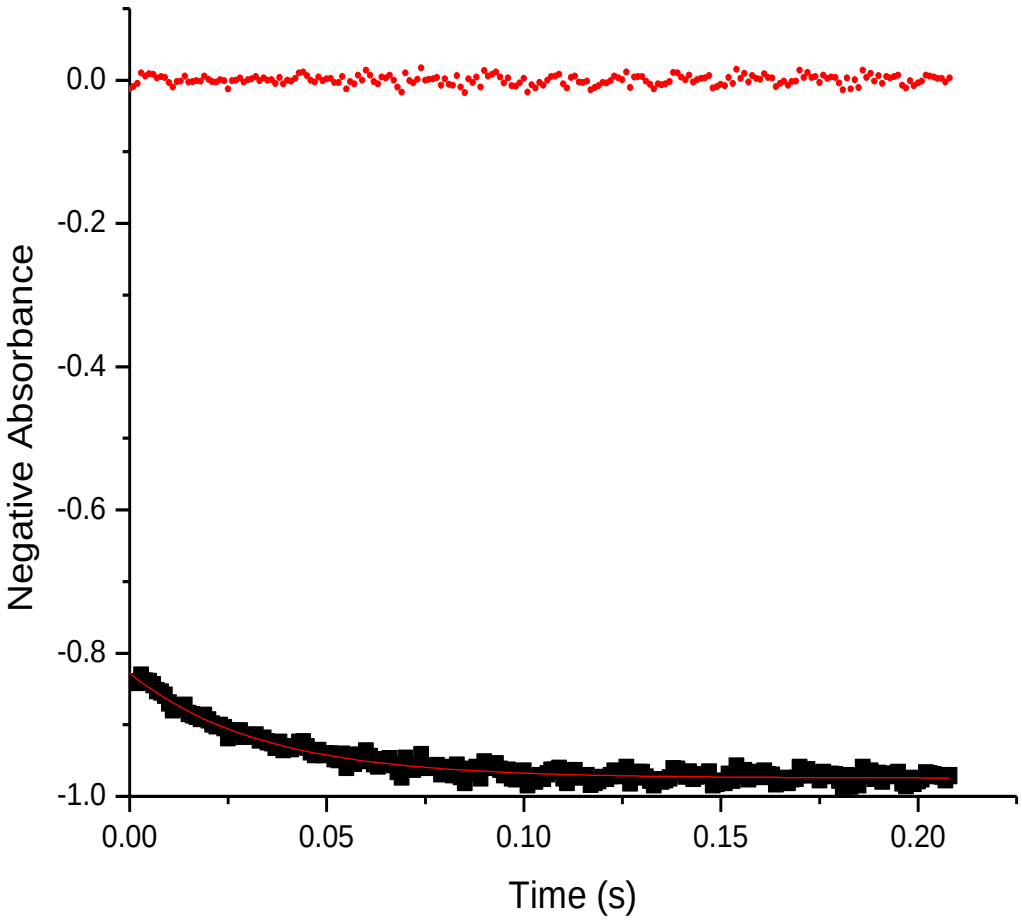

Figure 3.19 Plot of the negative of the absorbance values against time for rHbII at a concentration of 61 μM of an oxygen solution. The red dots represent a residual plot for the experimental data set. The red line represents the exponential decay analysis which is described by the following equation, $y = 0.1465\, e^{(-30.40t)} - 0.974$

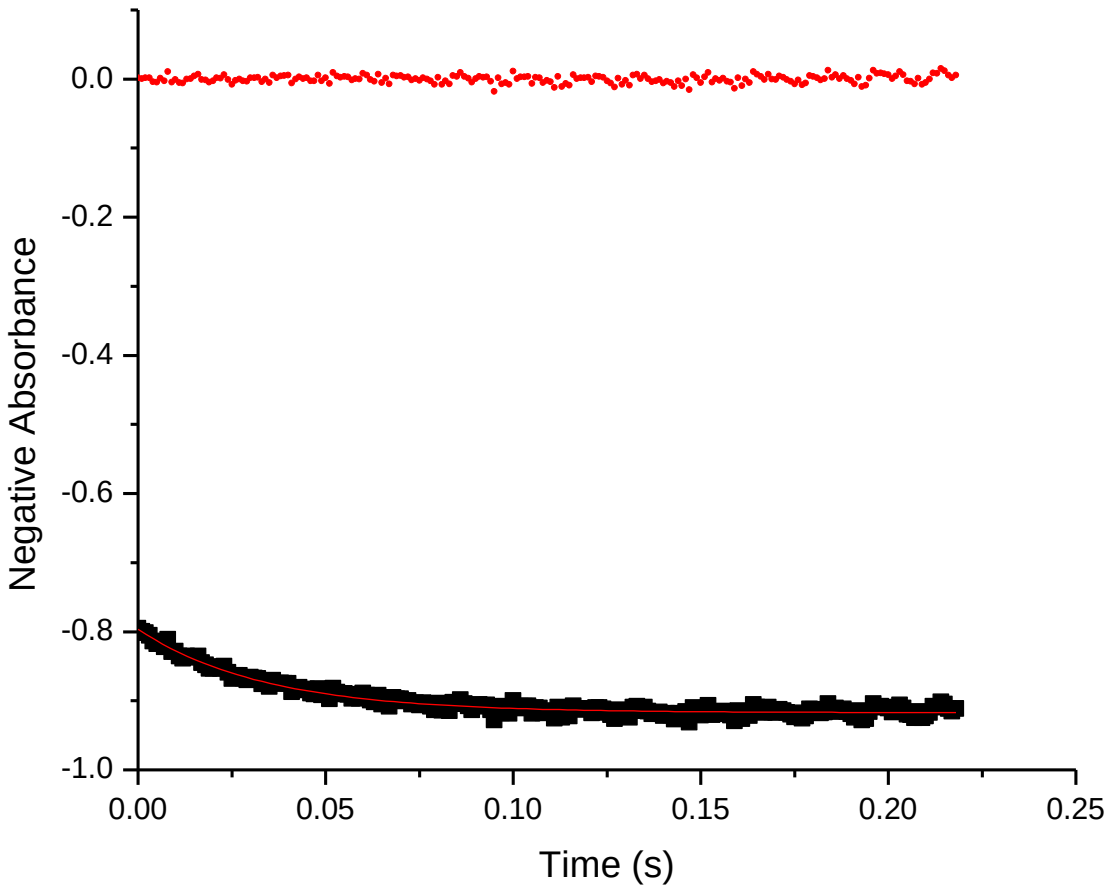

Figure 3.20 Plot of the negative of the absorbance values against time for rHbII at a concentration of 23 μM of an oxygen solution. The red dots represent a residual plot for the experimental data set. The red line represents the exponential decay analysis which is described by the following equation, $y = 0.1205\, e^{(-29.67t)} - 0.9172$

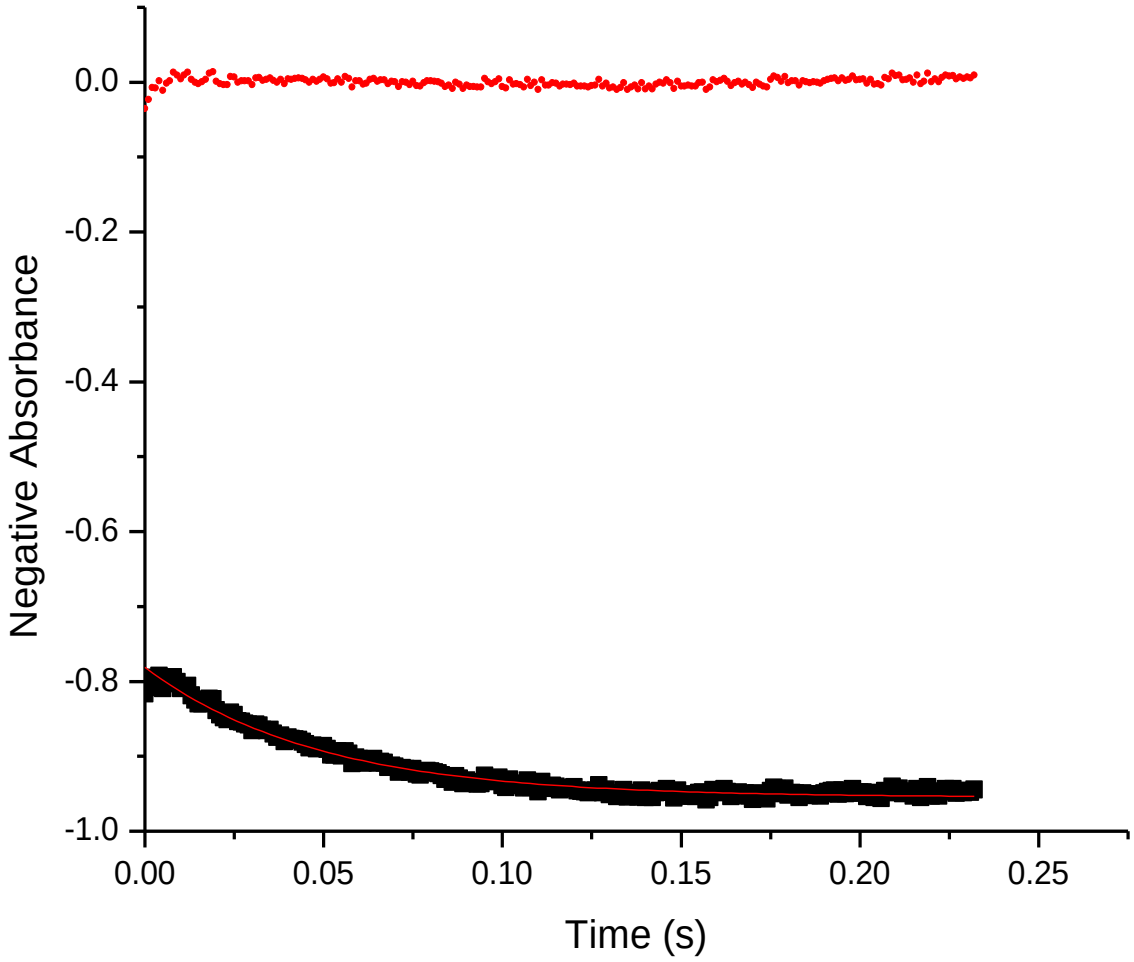

Figure 3.21 Plot of the negative of the absorbance values against time for rHbII at a concentration of 10 μM of an oxygen solution. The red dot represents a residual plot for the experimental data set. The red line represents the exponential decay analysis which is described by the following equation, $y = 0.1738\, e^{(-20.82t)} - 0.9547$

Table 3.6: Values of the pseudo first order rate constant, *k'*, obtained from the first order exponential decay analysis for HbII at different O_2 concentrations.

[O_2]	wtHbII	rHbII
325 μM	97.09 s^{-1}	83.06 s^{-1}
141 μM	52.89 s^{-1}	53.50 s^{-1}
61 μM	28.27 s^{-1}	30.40 s^{-1}
23 μM	35.77 s^{-1}	29.67 s^{-1}
10 μM	24.27 s^{-1}	20.82 s^{-1}

The second order rate constant (k_{on}) was obtained from the slope of the plot of the pseudo first order constant (k_{obs}) against O_2 concentration. Figure 3.22 illustrates the plot of *k'* versus [O_2] concentration for the wtHbII and the rHbII. For wtHbII, the k_{on} value obtained was 0.22 x 10^6 $M^{-1}s^{-1}$ and 0.19 x 10^6 $M^{-1}s^{-1}$ for recombinant HbII. The rapid entrance of the O_2 to the ligand-binding site can be explained by the conformational structure of the heme pocket. Resonance Raman studies suggest that the reduction of the heme cavity of HbII may help to stabilize the HbII-O_2 moiety once O_2 binds the heme iron center by forming hydrogen bonding interactions with Gln(E7) and Tyr(B10) (Gavira et al., 2008). Furthermore, the k_{on} value for the recombinant HbII is comparable with that reported by Kraus and Wittenberg (1990) for the wild type HbII of 0.390 x 10^6 M^{-1} s^{-1}. This small difference between the values may be attributed to the additional amino acid and histidine tag presented in the experiments.

3.6.2 Oxygen dissociation rate constant for rHbII

The dissociation of oxygen from rHbII was performed to characterize the protein. The disappearance of the 414 nm band and the appears of the 432 nm band were monitored in a UV-Vis spectrophotometer in the kinetic mode during 1 hr. The dissociation of the O_2 from the distal environment of the heme pocket follows a first order kinetics and the rate of this reaction is expressed as k_{off}[HbIIO_2]. The obtained data were analyzed using the Origin Pro 8.0 software, to determine the k_{off} value.

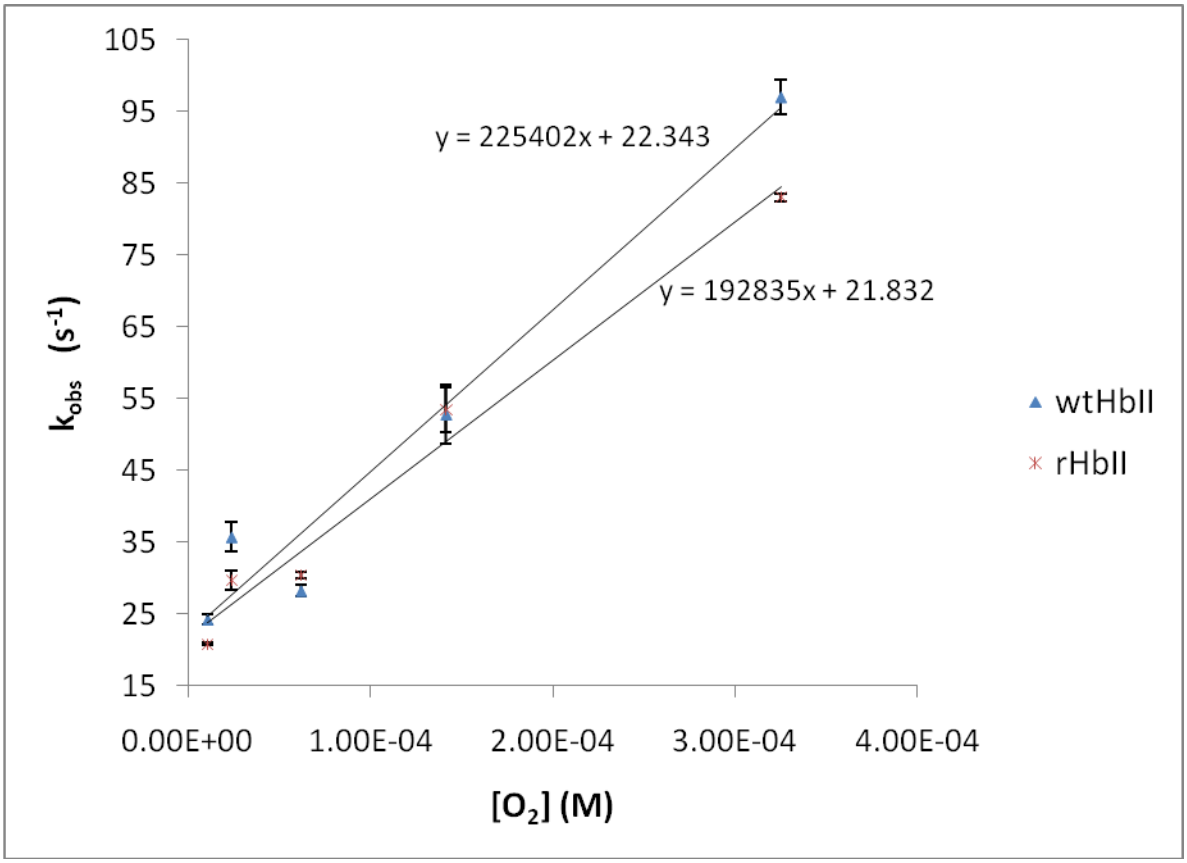

Figure 3.22 Plot of *k′* versus [O_2] concentration for the wtHbII and the rHbII. The k_{on} was obtained from the slope of the line.

For this analysis, the mathematical fit used to find the rate constant was the first order exponential decay analysis represented by the equation $y = A_1 \exp^{(-t1/x)} + y_0$, where 1/x is the first order decay constant (k_{off}), and the y_0 represent the A_∞. Table 3.5 shows the first order exponential decay analysis obtained for wtHbII and rHbII. Figure 3.23 display the experimental kinetic data and the first order exponential decay analysis for wtHbII-O_2 and rHbII-O_2. The dissociation rate constant (k_{off}) was determined from the slope (1/x) of the first order exponential equation. The first order rate constant, k_{off}, obtained was $0.0558s^{-1}$ for wild type HbII and $0.0526s^{-1}$ for rHbII.

Table 3.5: Summary of the first order exponential decay analysis for wtHbII and rHbII and the k_{off} obtained.

	wtHbII	**rHbII**
First order exponential decay analysis	$y = 0.14499 \exp^{(-t/17.935)} + 0.54561$	$y = 0.13819\exp^{(-t/19.012)} + 0.13819$
k_{off}	$0.0558s^{-1}$	$0.0526s^{-1}$

As expected, the dissociation rate constant was slow due the stable chemical bond between the O_2 and the tyrosine residue (Pietri, et al., 2005). It was demonstrated by X-Ray crystallography and Resonance Raman data of the wtHbII-O_2 complex that the protein form strong hydrogen bonds between the iron and the oxygen molecule. Also the data shows that exist a hydrogen network between Gln(E7) and Tyr(B10) which stabilizes the binding of the oxygen to HbII and it controlling the oxygen dissociation rate (Gavira, et al., 2008). Furthermore, the k_{off} value for the recombinant HbII is comparable with that reported by Kraus and Wittenberg (1990) for the wild type HbII of $0.11s^{-1}$.

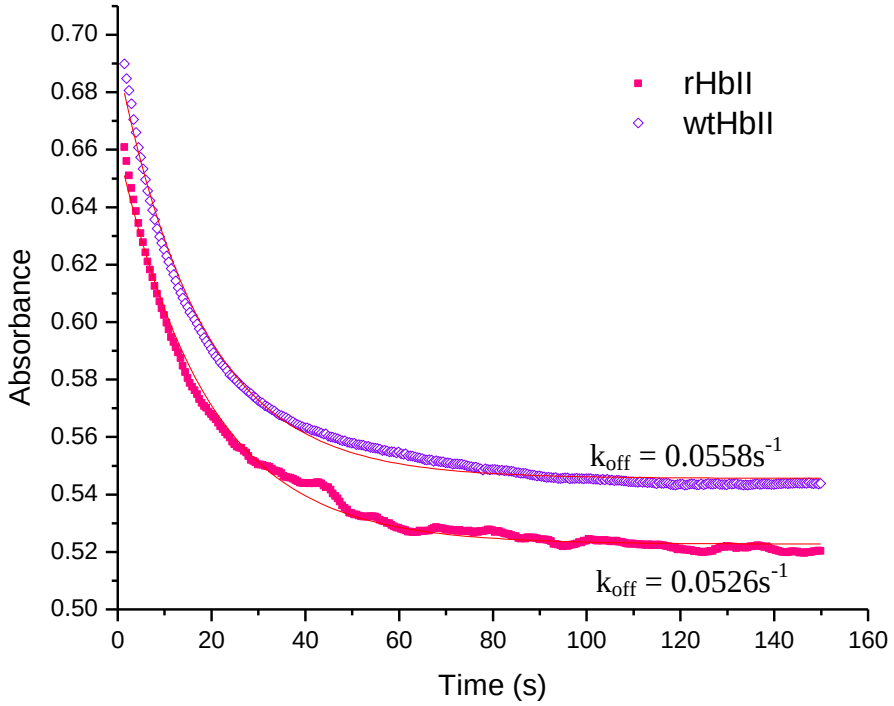

Figure 3.23 Kinetic trace for the O_2 dissociation from the recombinant HbII (..) and the wild type HbII (◊). The red line (---) represents the first order exponential decay analysis for each kinetic. A solution of 3 mg/mL of sodium dithionite was used to reduce the Fe and obtain the oxygen dissociation. The time courses of the kinetic were monitored at 414 nm in a UV-Vis spectrophotometer.

3.6.3 Autoxidation rate constant for rHbII

The autoxidation rate constant of HbII was measured using an UV-Vis spectrophotometer in the kinetic mode during 24 hours. The heme undergoes autoxidation from the oxy heme-Fe^{II} to the ferric heme-Fe^{III} form of the hemoglobin releasing oxygen as a superoxide ion. This process was monitored by the appears of the Soret band at 406 nm and the disappearance of the Soret band at 414 nm.

$$\text{Heme-Fe}^{II} + O_2 \longleftrightarrow \text{Heme-Fe}^{II}\text{-}O_2 \rightarrow \text{Heme-Fe}^{III} + O_2^{-} \qquad (12)$$

The autoxidation of rHbII follows a first order kinetics and the rate of this reaction is expressed as $k_{ox}[HbIIO_2]$. The obtained data were analyzed using the Origin Pro 8.0 software, to determine the k_{ox} value. For this analysis, the mathematical fit used to find the rate constant was the first order exponential decay analysis represented by the equation $y = A_1 \exp^{(-t/x)} + y_0$, where 1/x is the first order decay constant (k_{ox}), and the y_0 represent the A_∞. Figure 3.24 shows the kinetic trace for the autoxidation reaction (black dotes) of rHbII in which the absorbance is plotted vs a function of time. The first order exponential decay analysis obtained for rHbII was $y = 0.03096 \exp^{(-t/95873)} + 0.2070$. The autoxidation rate constant (k_{ox}) was determined from the slope (1/x) of the first order exponential equation. The first order rate constant, k_{ox}, obtained was $0.03744s^{-1}$ for rHbII. As expected, the kinetic trace for rHbII show that the autoxidation reaction is slower. The kinetic traces for rHbII show that the autoxidation reaction is slower. This result suggests that *L. pectinata* HbII may produce low concentrations of ROS (De Jesús-Bonilla et al., 2007).

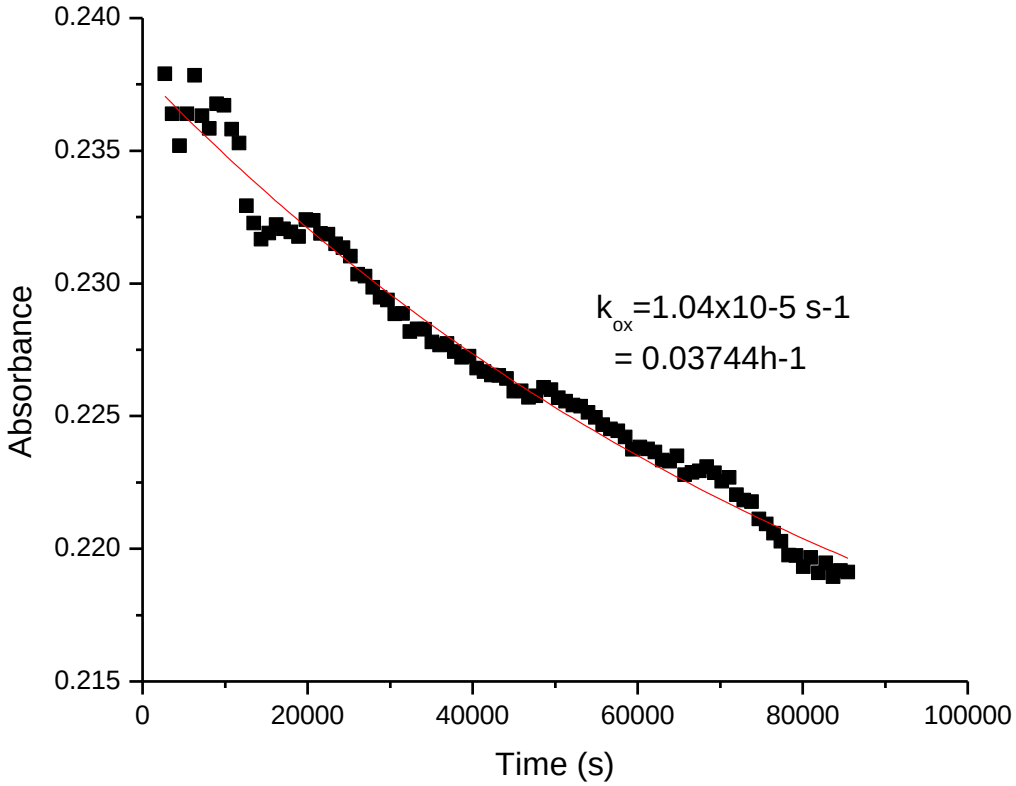

Figure 3.24 Kinetic trace for the autoxidation of the recombinant HbII. The red line (---) represents the first order exponential decay analysis for the kinetic. The time courses of the kinetic were monitored at 414 nm in a UV-Vis spectrophotometer.

Conclusions

The expression of recombinant hemoglobin II (rHbII) was achieved using hemin chloride. A maximum yield of 134.72 mg/L was obtained when BLi5 cell was used. The spectral properties of the protein were evaluated by exposition of the sample to oxidizing and reducing agents, as well as various distal ligands. Formation of the oxy, deoxy, carboxy, and metaquo complexes were observed, thereby indicating that rHbII have the capacity to bind different ligands at the distal binding site. These results also indicate that, similar to wtHbII and many Hbs, the recombinant HbII is able to response to oxidizing and reducing agents.

To further evaluate the O_2 association and dissociation reaction, kinetics of rHbII with the physiological relevant ligand were measured. The kinetic constants thus obtained were analogous to the wtHbII, suggesting that the recombinant protein maintained the oxygen-binding property of its wild type counterpart. Heme auto-oxidation, which is essential for the development of O_2 carriers, was also investigated for rHbII. Like wtHbII, the results show that the recombinant protein has a low auto-oxidation rate, thus making rHbII a good prototype for artificial blood.

Overall, this work sets the base for the development of HbII site-directed mutants to further improve the characteristics of a viable oxygen transporter. In addition, the development of HbII mutants can yield significant information about the role of the TyrB10 in this and other hemoglobins.

Reference

Alayash, A.I. (1999). Hemoglobin-based blood substitutes: oxygen carriers, pressor agents, or oxidants? *Nature Biotechnol.* 17: 545-549.

Alayash, A.I., Buehler, P.W. (2008). All hemoglobin-based oxygen carriers are not created equally. *Biochimica et Biophysica Acta*. 1784: 1378-1381.

Baldwin, A.L.(2004) Blood substitutes and redox responses in the microcirculation. *Antioxid redox Signal.* 6: 1019-1028.

Becker, C. (2001). Budgets may get bloodied. American Red Cross plans to raise average price of blood by nearly one-third. *Modern Healthcare.* 31-38.

Burmester, T., Weich, B. & Reinhardt, T.H. (2000). "A vertebrate globin expressed in the brain". *Nature.* 407: 520-523.

Chang, T.M.S. (2003). Future generations of red blood cell substitutes. *J. Inter. Med.* 253: 527-535.

Collazo, E., Pietri, R., De Jesús-Bonilla, W., Ramos, C., Del Toro, A., León, R.G., et al. (2004). Functional characterization of the purified holo form of hemoglobin I from *Lucina pectinata* overexpressed in Escherichia coli. *Protein J.* 23: 239-245.

De Jesus-Bonilla, W., Jia, Y., Alayash, A.I. and López-Garriga, J. (2007). Heme pocket geometry of *Lucina pectinata* hemoglobin II restricts nitric oxide and peroxide entry: A model of ligand control for the design of a stable oxygen carrier. *Biochemistry*. 46: 10451-10460.

De Jesus-Bonilla, W., Cruz, A., Lewis, A., Cerda, J., Bacelo, D.E., Cadilla, C.L. and Lopez-Garriga, J. (2006). Hydrogen-bonding conformations of tyrosine B10 tailor the hemeprotein reactivity of ferryl species. *J. Biol. Inorg. Chem*. 11: 334-342.

Dimino, M. L. & Palmer, A. F. (2007). Hemoglobin-based O_2 carrier O_2 affinity and capillary inlet pO2 are importaant factors that influence O_2 transport in a capillary. *Biotechnol. Prog*. 23: 921-931**.**

Egawa Tsuyoshi ; Yeh Syun-Ru. (2005). Structural and functional properties of hemoglobins from unicellular organisms as revealed by resonance raman spectroscopy. *Journal of Inorganic Biochemistry*. 99: 72-96.

Everts S. (2009). Artificial Blood. *Chemical & Engineering News*. 87: 52-55.

Gavira, J.A., De Jesús, W., Camara-Artigas, A., López-Garriga, J. and García-Ruiz, J.M. (2006). Capillary crystallization and molecular-replacement solution of haemoglobin II from the clam *Lucina pectinata*. *Acta Cryst*. F62: 196-199.

Gavira, J.A., Cámara-Artigas, A., De Jesús-Bonilla, W., López-Garriga, J. Lewis, A., Pietri, R., Yeh, S.R., et al., (2008). Structure and ligand selection of hemoglobin II from *Lucina pectinata*. *J. Biol. Chem.* 283: 9414-9423.

Goorha, B.YK., Deb, M.P., Chatterjee, L.C.T., Dhot, C.PS., Prassad, B.RS. (2003). Artificial Blood. *MJAFI*. 59: 45-50.

Herold, S. & Rock, G. (2003). Reactions of deoxy-, oxy-, and methemoglobin with nitrogen monoxide. Mechanistic studies of the S-nitrosothiol formation under different mixing conditions. *J. Biol. Chem.* 278*:* 6623-6634.

Jia, Y., Wood, F., Menu, P., Faivre, B., Caron, A., and Alayash, A.I. (2004). Oxygen binding and oxidation reactions of human hemoglobin conjugated to carboxylate dextran. *Biochim. et Biophys. Acta*. 1672: 164– 173.

Jung, Y., Kwak, J. and Lee, Y. (2001). High-level production of heme-containing holoproteins in *Escherichia coli*. *Appl Microbial Biotechnol*. 55: 187-191.

Kraus, D.W., and Wittenberg, J.B. Hemoglobins of the *Lucina pectinata*/Bacteria Symbiosis. I. (1990). Molecular properties, kinetics and equilibria of reactions with ligands. *J. Biol. Chem*. 265: 16043-16053.

Leon, R.G., Munier-Lehmann, H., Barzu, O., Baudin-Creuza, V., Pietri, R., Lopez-Garriga, J., and Cadilla, C.L. (2004). High-level production of recombinant sulfide-reactive hemoglobin I from *Lucina pectinata* in *Escherichia coli*: High yields of fully functional holoprotein synthesis in the BLi5 E. coli strain, *Protein Expr. Purif.* 38 (2), 184-195.

Mackenzie, Colin. Synthetic Blood: Myth or Reality?. (2005). *ITACCS*. 13-17.

Mozzarelli, A. (2008). Hemoglobin-based oxygen carriers as blood substitutes. *Biochimica et Biophysica Acta*. 1748: 1363-1364.

Natanson, C., Kern, S.J., Lurie, P., Banks, S.M., Wolfe, S.M. (2008). Cell-Free Hemoglobin-Based Blood Substitutes and Risk of Myocardial Infraction and Death. *JAMA*. 299: 2304-2312.

Ouellet, H., Ranguelova, K., Labarre, M., Wittenberg, J.B., Wittenberg, B.A., Magliozzo, R.S. & Guertin, M. (2007). Reaction of *Mycobacterium tubeculosis* truncated hemoglobin O with hydrogen peroxide: evidence for peroxidatic activity and formation of protein-based radicals. *J. Biol. Chem.* 282: 7491-7503.

Pietri, R., Granell, L., Cruz, A., De Jesús, W., Lewis, A., Leon, R., Cadilla, C.L. and López-Garriga, J. (2005). Tyrosine B10 and heme-ligand interactions of *Lucina pectinata* hemoglobin II: control of heme reactivity. *Biochimica et Biophysica Acta*. 1747: 195-203.

Rabinovici, R. (2001). The Status of Hemoglobin-Based Red Cell Substitutes. *IMAJ*. 3: 691-697.

Rosado-Ruiz, T., Antommattei-Pérez, F.M., Cadilla, C.L. and López-Garriga, J. (2001). Expression and Purification of Recombinant Hemoglobin I from Lucina pectinata. *J. Prot. Chem.* 20: 311-315.

Rousselot, M., Delpy, E., Drieu La Roche, C., Lagente, V., Pirow, R., Rees, J.F., et al., (2006). *Arenicola marina* extracellular hemoglobin: a new promising blood substitute. *Biotechnol. J.* 1: 333-45.

Schechter, A.N. (2008). Hemoglobin research and the origins of molecular medicine. *Blood*. 112: 3927-3938.

Spahn, D.R., Kocian, R. (2005) Artificial O_2 carriers: status in 2005. *Curr. Pharm. Des*. 2099-4114.

Squires, Jerry E. (2002). "Artificial Blood." *Science*. 1002: 1004-1005.

Tinmouth, A.T., McIntyre, L.A. & Fowler, R.A. (2008). Blood conservation strategies to reduce the need for red blood transfusion in critically ill patients. *CMAJ.* 178: 49-57

Torres-Mercado, E., Renta, J.Y., Rodríguez, Y., López-Garriga, J. & Cadilla, C. L. (2003). The cDNA-derived amino acid sequence of hemoglobin II from *Lucina pectinata*. *J. Prot. Chem.,* 22: 683-690.

Weickert, M.J., Pagratis, M., Curry, S.R., and Blackmore, R. (1997). Stabilization of apoglobin by low temperature increases yield of soluble recombinant hemoglobin in Escherichia coli**.** *Appl. Environ. Microbial*. 63: 4313-4320.

Winslow, R.M. (2008). Cell-free oxygen carriers: Scientific foundations. Clinical development, and new directions. *Biochimica et Biophysica Acta*. 1784: 1382-1386.

Yeh, L.H., Alayash, A.I. (2003) *J. Intern. Med.* 253: 518-526.